PERGAMON

Planetary and Space Science 49 (2001) 1067–1088

Planetary and Space Science

www.elsevier.com/locate/planspasci

Origin of the main auroral oval in Jupiter's coupled magnetosphere–ionosphere system

S.W.H. Cowley *, E.J. Bunce

Department of Physics and Astronomy, University of Leicester, University Road, Leicester LE1 7RH, UK

Received 4 September 2000; received in revised form 1 November 2000; accepted 14 November 2000

Abstract

We show that the principal features of the main auroral oval in the jovian system are consistent with an origin in the magnetosphere–ionosphere coupling currents associated with the departure of the plasma from rigid corotation in the middle magnetosphere, specifically with the inner region of field-aligned current directed upwards from the ionosphere to the magnetosphere. The features we refer to include its location, its continuity in local time, its width, and the precipitating particle energy flux and auroral luminosity. A simple empirical model of the field and flow in the middle magnetosphere is used to estimate the field-aligned currents flowing into and out of the equatorial current sheet associated with the breakdown of corotation. The models indicate that the current flows outwards from the ionosphere into the current sheet through most of the middle magnetosphere. Mapped to the ionosphere, the upward field-aligned current density is of order $\sim$1 μA m^{-2}, confined to circumpolar annular rings around each pole of latitudinal width $\sim 1^\circ$ ($\sim$1000 km), centred near $\sim 16^\circ$ dipole latitude. The upward current is carried principally by downward-precipitating magnetospheric electrons from the tenuous hot plasma which extends outside the cooler denser equatorial plasma sheet to high latitudes. For reasonable observed values of the magnetospheric electron parameters it is found that such currents require the existence of field-aligned voltages of order $\sim$100 kV. The auroral primaries are thus $\sim$100 keV electrons, consistent with deep penetration of the jovian atmosphere and low-altitude auroras, as observed. The peak ionospheric energy flux associated with the accelerated precipitating electrons is of order $\sim$0.1–1 W m^{-2}, sufficient to drive a UV aurora of 1–10 MR at $\sim$20% conversion efficiency. In addition, to produce the current, the acceleration region must extend in altitude typically above ~ 3–$4R_J$. The spatially extended energetic auroral electron beams so formed are suggested to form a principal source of free energy for non-Io-related radio emissions. An important implication of the model is that the main oval auroras and radio emissions will respond principally to the dynamic pressure of the solar wind, in the sense of anticorrelation.

1. Introduction

An important new source of information concerning the dynamics of the jovian magnetosphere has recently emerged via the availability of highly resolved images of jovian auroras. Images of this nature have been obtained at IR wavelengths from ground-based telescopes (e.g. Satoh et al., 1996), at UV wavelengths from the Hubble Space Telescope (e.g. Prangé et al., 1998; Clarke et al., 1998), and most recently and at highest spatial resolution in the visible by the Galileo orbiter (Vasavada et al., 1999). The IR auroras represent mainly thermal emissions from the heated auroral atmosphere and ionosphere, while the UV and visible auroras are directly excited by the precipitating magnetospheric particle flux. Various regions of auroral emission have been reported from these studies, including variable diffuse emissions at highest latitudes in the polar cap, and patches and arcs near the feet of the Io field line. However, the most significant emission in terms of energy output arises from circumpolar bands around both northern and southern poles, consistently observed in all the above wave bands, which has been termed the "main auroral oval". This emission, though of variable width and intensity, appears to be essentially continuous in local time. It occurs at dipole co-latitudes of $\sim 15^\circ$, closer to the pole than the Io flux tube, and encircles the polar cap emission at highest latitudes. Magnetic modelling studies reported by the above authors indicate that it lies on field lines which map to the equator beyond $\sim 20R_J$, and thus to the region of the jovian middle magnetosphere current sheet (e.g. Smith et al., 1976; Acuña et al., 1983). The emission is very narrow in latitudinal extent, but very bright. The overall width is $\sim$1000 km (i.e. $\sim 1^\circ$ of latitude), with a brightness above $\sim$100 kR at visible and UV wavelengths (Prangé et al., 1998; Vasavada et al.,

* Corresponding author. Tel.: 0044-116-223-1331; fax: 0044-116-252-3555.

E-mail address: swhc1@ion.le.ac.uk (S.W.H. Cowley).

0032-0633/01/$ - see front matter
PII: S0032-0633(00)00167-7

1999). However, peak emissions within this band can have a brightness up to several MR, confined to regions of width a few ~100 km or below. Assuming a ~20% conversion efficiency (Prangé et al., 1998), the precipitating particle energy input is thus estimated to lie typically in the range from a few tens to a few hundred of mW m^{-2}. Estimates of the emission altitude vary from ~250 km above the 1 bar level for the optical emission (Vasavada et al., 1999), to ~300–500 km above the 1 bar level for the UV emission (Prangé et al., 1998). The implication of such low altitudes is that the precipitating primaries, assumed electrons, must include particles of very high energies, from several tens to several hundreds of keV, in agreement with the results of studies based on the UV emission spectra (Ajello et al., 1998).

Previous theoretical discussion of the origins of jovian auroral precipitation has mainly focussed on wave-driven pitch-angle diffusion of hot magnetospheric plasma (Thorne, 1983). Although wave amplitudes may be sufficient to fill the loss cone and hence to produce significant precipitation, the resulting ionospheric energy fluxes are found typically to be ~0.1–1 mW m^{-2}. Such conclusions were most recently confirmed by Tsurutani et al. (1997), who examined the hypothesis that the main oval is formed by wave diffusion of magnetospheric plasma in the magnetopause boundary layer. Using Ulysses data, they found that wave amplitudes were sufficient to maintain keV electrons and keV–MeV protons at the strong pitch angle diffusion (filled loss-cone) limit, but that the resulting precipitated energy fluxes were too low by ~2–3 orders of magnitude to account for the main oval emissions.

Jovian auroras have also been associated with field-aligned current systems which couple the magnetosphere and ionosphere, particularly those associated with the Alfvén waves which are formed downstream of Io in the corotating magnetospheric flow, and which propagate along the field lines to the ionosphere (e.g. Hill et al., 1983; Kopp et al., 1998). On a larger scale, Isbell et al. (1984) have discussed the excitation of field-aligned currents and related aurora by the interaction between the solar wind and a rapidly rotating magnetised planet. They point out that flux tubes in the magnetopause boundary layer which are transported downstream from the planet and into the tail by the input of solar wind momentum will be twisted by planetary rotation, thus forming annular zones of field-aligned current which flow toward and away from the planet. Such a mechanism might operate on polar cap field lines which map, in the main, to the magnetospheric tail at large distances from the planet. However, it does not seem an appropriate starting point to describe the main jovian auroral oval which, as mentioned above, seems clearly to map deeper inside the magnetosphere, to the region of the middle magnetosphere current sheet. Indeed, Gérard et al. (1994) have suggested a physical link between the UV aurora and field-aligned current sheets observed at jovicentric distances of ~15–20R_J during the dusk outbound pass of the Ulysses spacecraft (Dougherty et al., 1993).

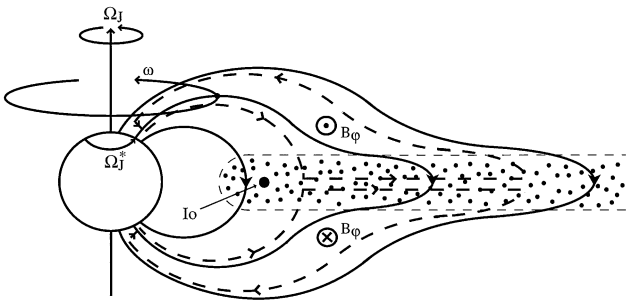

Fig. 1. Sketch of a meridian cross-section through the jovian magnetosphere, showing the principal features of the inner and middle magnetosphere regions. The arrowed solid lines indicate magnetic field lines, which are distended outwards in the middle magnetosphere region by azimuthal currents in the plasma sheet. The plasma sheet plasma originates mainly at Io, which orbits in the inner magnetosphere at ~6R_J, liberating ~10^3 kg s^{-1} of sulphur and oxygen plasma. This plasma is shown by the dotted region, which rotates rapidly with the planetary field due to magnetosphere–ionosphere coupling while more slowly diffusing outwards. Three separate angular velocities associated with this coupling are indicated. These are the angular velocity of the planet Ω_J, the angular velocity of a particular shell of field lines ω, and the angular velocity of the neutral upper atmosphere in the Pedersen layer of the ionosphere, Ω_J^*. The latter is expected to lie between ω and Ω_J because of the frictional torque on the atmosphere due to ion-neutral collisions. The oppositely directed frictional torque on the magnetospheric flux tubes is communicated by the current system indicated by the arrowed dashed lines, shown here for the case of sub-corotation of the plasma (i.e. $\omega \leqslant \Omega_J$). This current system bends the field lines out of meridian planes, associated with azimuthal field components B_φ as shown.

In open discussion at the Magnetospheres of the Outer Planets meeting in Paris, August 1999, V.M. Vasyliunas suggested that the main oval is related to the magnetosphere–ionosphere coupling current system associated with the breakdown of corotation in the middle magnetosphere, specifically with the region of upward field-aligned current (see Fig. 1, to be discussed further below). A prediction of this nature had been made much earlier by Kennel and Coroniti (1975), in relation to the coupling of angular momentum between the planet and magnetosphere in a solar wind-like radial outflow plasma model which was then under discussion. This suggestion has the initial virtues that it is immediately consistent with both the observed longitudinal continuity of the aurora, and the magnetospheric mapping. Observations of the jovian plasma flow, albeit limited at present, suggest that departures from rigid corotation begin at equatorial distances of ~20R_J (Belcher, 1983; Sands and McNutt, 1988). (We are referring here, of course, to the departures from corotation associated with outward radial transport of the iogenic plasma, and not to the localised departures in the vicinity of Io's orbit at ~6R_J which are instead associated with the ionisation of neutral gas and pick-up by the flow (e.g. Brown, 1994)). In this paper we therefore quantitatively investigate this suggestion, specifically with regard to the amplitude and width of the field-aligned currents, and the conditions under which

they may be carried by the magnetospheric plasma. In the next section we therefore employ a simple empirical model of the middle magnetosphere, based on observations, to evaluate the amplitude and extent of the field-aligned currents. In Section 3 we then consider how these currents are carried, and show that large $\sim$100 kV field-aligned voltages are required along the auroral field lines, thus also resulting in large precipitated particle energy fluxes.

2. Breakdown of corotation and field-aligned currents

2.1. Physical background

In this section we present a simple empirical model of the field and flow in the middle magnetosphere, and use it to estimate the form and magnitude of the field-aligned currents which couple the magnetosphere and ionosphere in this region. We first discuss the physical background to the theory, and in Fig. 1 sketch a cross-section through the inner and middle magnetosphere showing the principal features. The plasma in the jovian magnetosphere originates principally from the moon Io, which orbits at a radial distance of $\sim 6R_J$, deep within the magnetosphere. The plasma consists mainly of sulphur and oxygen ions, together with equal numbers of electrons, and is confined to a near-equatorial toroidal plasma sheet (the dotted region in Fig. 1) by the centrifugal action of the near-corotating plasma flow. This plasma diffuses slowly outwards into the equatorial middle magnetosphere via centrifugally driven flux-tube interchange motions whose details are not thoroughly understood as yet, and is eventually lost down-tail, again via processes which are not at present well-determined. Here we use the term "middle magnetosphere" to describe the region of field lines which pass through the equatorial plasma sheet. This plasma carries a strong equatorial azimuthal current associated with radial stress balance, which thus distends the field lines in this region outwards from the planet, as shown in the figure.

As the iogenic plasma diffuses outward, its angular velocity, which is close to rigid corotation with the planet in the source region, tends to fall. If there is no torque on the plasma, conservation of angular momentum indicates that the azimuthal speed of the plasma will fall with radial distance as ρ^{-1}, such that the angular velocity will fall as ρ^{-2}. However, when the angular velocity of the flux tubes fall below the angular velocity of the planet, a differential velocity exists between the neutral particles in the upper atmosphere which rotate with the planet to a first approximation, and the charged particles in the ionosphere which rotate with the flux tubes. Collisions between ions and neutral particles in the Pedersen-conducting layer of the ionosphere will then form a frictional torque on the flux tubes which tends to spin them back up towards corotation, while the equal and opposite torque on the neutral atmosphere tends at the same time to reduce the angular velocity of the upper atmospheric gas (Kennel and Coroniti, 1975; Huang and Hill, 1989). In the steady state, Hill (1979) first showed theoretically that the ionospheric torque is sufficient to maintain near-rigid corotation within a distance of a few tens of jovian radii in the equatorial plane, depending on the ionospheric Pedersen conductivity (directly related to the ion-neutral collisions) and the mass outflow rate of the iogenic plasma. Beyond this distance, the ionospheric torque becomes increasingly ineffective, such that the angular velocity then falls increasingly away from rigid corotation, as ρ^{-2} at large distances.

The ionospheric frictional torque is communicated to the collisionless magnetospheric plasma by the magnetic field, which is distorted out of magnetic meridian planes into a "lagging" configuration. The field distortion is associated with azimuthal field components which are directed opposite to corotation north of the equatorial plasma sheet, and in the same direction as corotation south of the plasma sheet, as observed (e.g. Smith et al., 1976; Khurana and Kivelson, 1993; Bunce and Cowley, 2001), and as shown in Fig. 1. The related current system is shown in Fig. 1 by dashed lines, following the prior discussions of Hill (1979) and Vasyliunas (1983). Pedersen currents flow equatorward in both hemispheres, and close in outward radial currents in the plasma sheet via a large-scale system of field-aligned currents which flow in the tenuous plasma between the ionosphere and the plasma sheet. The Pedersen current in the ionosphere is associated with a $\mathbf{j} \times \mathbf{B}$ force directed opposite to the rotation of the planet which balances the frictional force of the neutral atmosphere on the ions. The force of the ions on the neutral particles, which tends to de-spin the atmosphere, is thus equal to the $\mathbf{j} \times \mathbf{B}$ force of the Pedersen current. The outward radial current in the equatorial plasma sheet is associated with a $\mathbf{j} \times \mathbf{B}$ force in the sense of planetary rotation, which tends to accelerate the magnetospheric plasma towards corotation with the planet. These forces are such that if we consider any given flux tube, the torque about the spin axis which tends to de-spin the atmosphere (summed over northern and southern hemispheres) is equal and opposite to the "spin-up" torque on the equatorial plasma. The circuit is then completed by field-aligned currents which are directed outwards from the ionosphere into the magnetospheric plasma sheet in the inner part of the region where the angular velocity of the plasma begins to depart from rigid corotation, while reversing in sense at larger distances in the outer part of the plasma sheet (Hill, 1979; Vasyliunas, 1983). The main auroral oval is suggested here to correspond to the former of these field-aligned currents.

Our initial task is to estimate the form and magnitude of these field-aligned currents, employing for the purpose a simple empirical model of the field and flow. First of all, however, we outline the basic theory, following the previous discussions of Vasyliunas (1983) and Bunce and Cowley (2001).

2.2. Basic theory

We consider an axisymmetric magnetic field (at least locally) whose principal components in cylindrical (ρ, φ, z) coordinates are the poloidal components B_ρ and B_z, but where there is also a B_φ component associated with field bending out of meridian planes, as mentioned above. The curl of B_φ gives the field-aligned current density in the region between the ionosphere and the plasma sheet where the field-perpendicular currents are negligible, and in this region $\rho B_\varphi =$ constant along the field lines. The poloidal field is described in terms of the vector potential $\mathbf{A}$ (where $\mathbf{B} = \text{curl}\,\mathbf{A}$) by the expressions

$$B_\rho = -\frac{\partial A_\varphi}{\partial z} \tag{1a}$$

$$B_z = \frac{1}{\rho}\frac{\partial(\rho A_\varphi)}{\partial \rho}, \tag{1b}$$

which thus only involve the azimuthal component, A_φ. The flux function for such a field is given by $F = \rho A_\varphi$, and is such that F is constant on a field line (i.e. $(\mathbf{B}\cdot\nabla)F = 0$). The surface $F =$ constant thus defines an azimuthally symmetric "shell" of field lines passing from the southern ionosphere, through the equator, to the northern ionosphere. Knowledge of F thus allows us to map field lines between the equatorial current sheet and the ionosphere. Specifically, it allows us to calculate in a simple manner the ionospheric co-latitude of a field line which passes through the equator at a given radial distance. In general, F consists of two terms, the first due to the internal field of the planet, approximated here by the dipole term alone, while the second is due to external currents, principally the azimuthal currents in the equatorial current sheet in the middle magnetosphere. In the ionosphere, the planetary dipole term is overwhelmingly dominant, given by

$$F_{\text{dip}} = B_J \rho^2 \left(\frac{R_J}{r}\right)^3, \tag{2}$$

where r is the jovicentric radial distance, B_J is the jovian equatorial magnetic field strength (taken to be 4.28×10^5 nT in conformity with the VIP 4 internal field model of Connerney et al. (1998)), and R_J is Jupiter's radius (taken to be 71,373 km). The absolute value of F has been fixed by taking $F = 0$ on the magnetic axis. Putting $r \approx R_J$ to a sufficient approximation in Eq. (2) then gives the ionospheric value of the flux function

$$F_i \approx B_J \rho_i^2 = B_J R_J^2 \sin^2\theta_i, \tag{3}$$

where ρ_i is the perpendicular distance from the magnetic axis, and θ_i is the magnetic co-latitude. In the equatorial plane the flux function F_e is given by integration of Eq. (1b)

$$\frac{dF_e}{d\rho_e} = \rho_e B_{ze}, \tag{4}$$

where B_{ze} is the north–south component of the magnetic field threading through the current sheet (negative in the case of Jupiter), and ρ_e is the radial distance from the magnetic axis. The field B_{ze} also consists of dipole and current sheet contributions, the specific model for which employed here will be described below. Mapping between the ionosphere and equatorial plane is then achieved simply by writing $F_i(\theta_i) = F_e(\rho_e)$.

In the theory we distinguish three separate angular velocities with respect to an inertial (non-rotating) frame, as indicated in Fig. 1. The first is the angular velocity of rotation of the planet, Ω_J, which we take for simplicity to be aligned with the magnetic axis ($\Omega_J \approx 1.76\times10^{-4}$ rad s^{-1}). We thus neglect the $\sim10^\circ$ tilt of the dipole axis relative to the spin axis, since this is not essential to the issues we wish to address. The effects of dipole tilt will be discussed further in Section 4. The second is the angular velocity ω of the plasma on the "shell" of magnetic field lines of a given value of F, which we take to be constant along the field lines in the steady state. That is, we assume that each flux shell rotates rigidly without time-dependent distortion, though in general the shells rotate differentially with respect to each other. Sub-corotation of the plasma, as expected, implies $\omega < \Omega_J$. The third is the angular velocity of the neutral atmosphere in the Pedersen conducting layer, Ω_J^*, which can differ from the angular velocity of the planet due to the torque induced by ion-neutral collisions, as mentioned above. In this case, we may anticipate that Ω_J^* will take a value which is intermediate between ω and Ω_J, such that formally we can write

$$(\Omega_J - \Omega_J^*) = k(\Omega_J - \omega), \tag{5}$$

for some $0 < k < 1$. The value of k is not well known at present, but preliminary results based on the JIM model of the coupled jovian ionosphere–thermosphere system (Achilleos et al., 1998), indicate that k may be as large as $\sim$0.5, or possibly higher (S. Miller, private communication, 2000).

Consideration of the continuity of the current in the magnetosphere–ionosphere coupling circuit in Fig. 1 shows that the current flowing in the two ionospheres on field lines of a given value of F in a given angular sector is equal to the current flowing in the equatorial plane on the same field lines in the same angular sector. Assuming for simplicity that conditions in conjugate ionospheres are identical thus yields

$$\rho_e i_{\rho e} = 2\rho_i i_{Pi}, \tag{6}$$

where ρ_e and ρ_i are (as above) the perpendicular distances of the field lines from the magnetic axis in the equatorial plane and in the ionosphere, respectively, $i_{\rho e}$ is the radial equatorial magnetospheric current intensity (A m^{-1}), integrated across the width of the plasma sheet, and i_{Pi} is the equatorward height-integrated ionospheric Pedersen current intensity. It is easily shown that under this condition, determined from current continuity, the torque about the magnetic axis on the equatorial plasma on a given magnetic flux tube is equal and opposite to the summed torques on the ionospheric plasma in the northern and southern hemispheres, as

indicated above. The ionospheric current intensity in each hemisphere is given by

$$i_{\mathrm{Pi}} = \Sigma_{\mathrm{P}} E_{\mathrm{i}}, \tag{7}$$

where Σ_{P} is the height-integrated ionospheric Pedersen conductivity, and E_{i} is the equatorward ionospheric electric field in the rest frame of the neutral atmospheric gas. Assuming the polar magnetic field to be near-vertical and equal to twice the equatorial field B_{J} in strength, the electric field is then given by

$$E_{\mathrm{i}} = 2 v_{\mathrm{i}} B_{\mathrm{J}} = 2(\Omega_{\mathrm{J}}^{*} - \omega)\rho_{\mathrm{i}} B_{\mathrm{J}}, \tag{8}$$

where v_{i} is the (westward) ion flow in the neutral atmosphere rest frame. The ionospheric Pedersen current intensity is therefore

$$\begin{aligned} i_{\mathrm{Pi}} &= 2\Sigma_{\mathrm{P}}(\Omega_{\mathrm{J}}^{*} - \omega)B_{\mathrm{J}}\rho_{\mathrm{i}} = 2(1-k)\Sigma_{\mathrm{P}}(\Omega_{\mathrm{J}} - \omega)B_{\mathrm{J}}\rho_{\mathrm{i}} \\ &= 2\Sigma_{\mathrm{P}}^{*}(\Omega_{\mathrm{J}} - \omega)B_{\mathrm{J}}\rho_{\mathrm{i}}, \end{aligned} \tag{9}$$

where we have used Eq. (5) to derive the second form on the RHS of Eq. (9). In the last form on the RHS we have (following Huang and Hill (1989)) introduced the "effective" Pedersen conductivity of the ionosphere

$$\Sigma_{\mathrm{P}}^{*} = (1-k)\Sigma_{\mathrm{P}}, \tag{10}$$

which is reduced from the true value by the factor $(1-k)$ due to the "slippage" of the neutral atmosphere from rigid corotation resulting from the ion-neutral collisional torque. Introducing Eq. (9) into Eq. (6) and using Eq. (3) then yields

$$\rho_{\mathrm{e}} i_{\rho\mathrm{e}} = 4\Sigma_{\mathrm{P}}^{*}(\Omega_{\mathrm{J}} - \omega)\rho_{\mathrm{i}}^{2} B_{\mathrm{J}} = 4\Sigma_{\mathrm{P}}^{*}(\Omega_{\mathrm{J}} - \omega)F_{\mathrm{i}}. \tag{11}$$

The magnitude and direction of the field-aligned currents flowing between the ionosphere and the equatorial plasma sheet are directly related to the radial variation of the quantity $\rho_{\mathrm{e}} i_{\rho\mathrm{e}}$, the equatorial radial current per radian of azimuth. In fact it is clear that since there is no source of radial current at the planet, the value of $\rho_{\mathrm{e}} i_{\rho\mathrm{e}}$ at a certain distance is equal to the integral of all the field-aligned current flowing into the current sheet up to that distance per radian of azimuth. We will return to this point at the end of this section. The condition $\mathrm{div}\,\mathbf{j} = 0$ then yields the following expression for the current density j_z flowing northwards out of the northern surface of the current sheet

$$j_z = -\frac{1}{2}\mathrm{div}(i_{\rho\mathrm{e}}\hat{\rho}) = -\frac{1}{2\rho_{\mathrm{e}}}\frac{\mathrm{d}}{\mathrm{d}\rho_{\mathrm{e}}}(\rho_{\mathrm{e}} i_{\rho\mathrm{e}}), \tag{12}$$

where we have assumed that an equal and opposite current also flows southward out of the southern surface of the current sheet, hence giving the factor of a half. Thus if $\rho_{\mathrm{e}} i_{\rho\mathrm{e}}$ is independent of distance, no current flows into or out of the current sheet from the "sides", and there is no field-aligned current. If, however, $\rho_{\mathrm{e}} i_{\rho\mathrm{e}}$ increases with distance, as expected in the inner part of the system, then current must flow from the ionosphere to the current sheet, so that j_z will be negative in the northern hemisphere. Correspondingly, if $\rho_{\mathrm{e}} i_{\rho\mathrm{e}}$ decreases with distance, then current must flow from the current sheet to the ionosphere, and j_z will be positive in the northern hemisphere. However, the quantity we require is not j_z directly, but the field-aligned current density per unit magnetic field. In the assumed absence of field-perpendicular currents in the region between the equatorial plasma sheet and the ionosphere, this quantity will be constant along the field lines in this region (i.e. it is a function of F), and thus allows us to map the field-aligned current into the ionosphere. In the equatorial plane we thus have from Eq. (12)

$$\frac{j_{||\mathrm{e}}}{B_{\mathrm{e}}} = \frac{j_{z\mathrm{e}}}{B_{z\mathrm{e}}} = -\frac{1}{2\rho_{\mathrm{e}} B_{z\mathrm{e}}}\frac{\mathrm{d}}{\mathrm{d}\rho_{\mathrm{e}}}(\rho_{\mathrm{e}} i_{\rho\mathrm{e}}), \tag{13}$$

and hence in general we find

$$\begin{aligned} \left(\frac{j_{||}}{B}\right) &= -\frac{1}{2\rho_{\mathrm{e}} B_{z\mathrm{e}}}\frac{\mathrm{d}}{\mathrm{d}\rho_{\mathrm{e}}}(\rho_{\mathrm{e}} i_{\rho\mathrm{e}}) = -\frac{2}{\rho_{\mathrm{e}} B_{z\mathrm{e}}}\frac{\mathrm{d}}{\mathrm{d}\rho_{\mathrm{e}}}(\Sigma_{\mathrm{P}}^{*}(\Omega_{\mathrm{J}} - \omega)F_{\mathrm{e}}) \\ &= -2\frac{\mathrm{d}}{\mathrm{d}F}(\Sigma_{\mathrm{P}}^{*}(\Omega_{\mathrm{J}} - \omega)F), \end{aligned} \tag{14}$$

where we have employed Eqs. (4) and (11). The last form makes it clear that $(j_{||}/B)$ is indeed a function of F alone, and thus constant on a field line between the equator and the ionosphere. The field-aligned current density in the ionosphere is thus given by

$$j_{||\mathrm{i}} = 2B_{\mathrm{J}}\left(\frac{j_{||}}{B}\right) = -\frac{4B_{\mathrm{J}}}{\rho_{\mathrm{e}} B_{z\mathrm{e}}}\frac{\mathrm{d}}{\mathrm{d}\rho_{\mathrm{e}}}(\Sigma_{\mathrm{P}}^{*}(\Omega_{\mathrm{J}} - \omega)F_{\mathrm{e}}). \tag{15}$$

We noted above that the value of $\rho_{\mathrm{e}} i_{\rho\mathrm{e}}$ at a certain radial distance is equal to the integral of all the field-aligned current flowing into the current sheet up to that distance, per radian of azimuth. That is, from Eq. (11)

$$I_{||} = -I_z = -2\int_0^{\rho_{\mathrm{e}}} j_z \rho_{\mathrm{e}}' \,\mathrm{d}\rho_{\mathrm{e}}' = \rho_{\mathrm{e}} i_{\rho\mathrm{e}} = 4\Sigma_{\mathrm{P}}^{*}(\Omega_{\mathrm{J}} - \omega)F_{\mathrm{e}}, \tag{16}$$

where we have included the current from both hemispheres. Near to the planet we expect $\omega \to \Omega_{\mathrm{J}}$, so that $(\Omega_{\mathrm{J}} - \omega) \to 0$, and $I_{||} \to 0$ as expected. With increasing distance, $(\Omega_{\mathrm{J}} - \omega)$ will increase towards Ω_{J}, while F_{e} will fall towards zero. In general, the product $4\Sigma_{\mathrm{P}}^{*}(\Omega_{\mathrm{J}} - \omega)F_{\mathrm{e}}$ will thus achieve a maximum value at a certain distance, and will then fall. The field-aligned current flows into the current sheet from both sides up to the distance of the maximum value, and then flows out again at larger distances. The total current per radian flowing in the circuit (both ionospheres combined) is thus given by the maximum value of $4\Sigma_{\mathrm{P}}^{*}(\Omega_{\mathrm{J}} - \omega)F_{\mathrm{e}}$. In a closed axisymmetric magnetosphere F_{e} would then go to zero (the value at the planet's pole) at the outer boundary of the system in the equatorial plane. In this case $4\Sigma_{\mathrm{P}}^{*}(\Omega_{\mathrm{J}} - \omega)F_{\mathrm{e}} \to 0$ at the boundary, and all the current that enters the sheet in the inner part exits the sheet in the outer part. In an open magnetosphere (i.e. a magnetosphere with an extended magnetic tail), however, F_{e} will not go to zero at the equatorial boundary, but to a finite value depending on the amount of open flux present in the system (the magnetic flux $\mathrm{d}\Phi$ per radian of azimuth between flux shells F and $F + \mathrm{d}F$ is just $\mathrm{d}\Phi = \mathrm{d}F$). In this case not all of the field-aligned current which flows into the current sheet in the inner part will

exit from the current sheet in the outer part. The remainder will then close back into the ionosphere via the outer boundary region where the equatorial current sheet terminates (i.e. the magnetopause and boundary layers if the current sheet terminates near the magnetopause).

2.3. Empirical model

In order to calculate $(j_{||}/B)$ as a function of distance in the equatorial plane from Eq. (14), and hence $j_{||\mathrm{i}}$ as a function of co-latitude in the ionosphere from Eq. (15), we thus need to specify the variation with distance in the equatorial plane of the effective Pedersen conductivity Σ_{P}^{*} at the feet of the field lines, the angular velocity of the plasma ω, and the flux function F_{e} and $B_{z\mathrm{e}}$ field (which are themselves connected via Eq. (4)). In constructing the model presented here our goal has been to consider only the simplest model consistent with observations which is needed to demonstrate the physical effects of interest. The first simplification we have made is thus to treat Σ_{P}^{*} as a constant, independent of latitude. This is undoubtedly not the case because the intense particle precipitation into the main auroral oval must significantly elevate the ionospheric densities and conductivities in this region relative to lower latitudes. However, essentially no information exists on this effect at present, and attempting to model the potentially complex relations between precipitation, conductivity, and plasma angular momentum is significantly beyond the scope of the simple estimations envisaged here. We thus take a constant value equal to 0.5 mho, a value recently found to be consistent with the observed azimuthal fields in the middle magnetosphere associated with the "lagging" field configuration (Bunce and Cowley, 2001). This value is a little higher than those usually considered (of a few tenths of a mho), but is taken to be representative of an ionosphere whose conductivity is somewhat elevated by auroral precipitation. However, the results derived here can readily be scaled over a reasonably broad range of conductivities to other assumed values, as will be mentioned below.

The second topic concerns the adoption of a simplified form representing the radial profile of the angular velocity of the plasma in the equatorial plane. Again, observational information is relatively sparse. As indicated above, thermal plasma observations during the pre-noon inbound passes of Voyagers 1 and 2 indicate near-rigid corotation in the inner part of the magnetosphere (except locally near Io's orbit as noted above), with $\omega/\Omega_{\mathrm{J}} \approx 0.8$ between 10 and $20R_{\mathrm{J}}$, falling to $\sim$0.5 at $\sim 40R_{\mathrm{J}}$ (Belcher, 1983; Sands and McNutt, 1988). At the larger distances of ~ 30–$50R_{\mathrm{J}}$ on the Voyager 2 inbound pass, values of $\omega/\Omega_{\mathrm{J}} \approx 0.5$–$0.6$ have also been derived from energetic ion anisotropies (Kane et al., 1995). Similarly, at ~ 50–$70R_{\mathrm{J}}$ on the pre-noon inbound Ulysses pass, values of $\omega/\Omega_{\mathrm{J}} \approx 0.2$ have been reported from thermal electron and energetic ion data (Phillips et al., 1993; Laxton et al., 1997). On the post-midnight outbound pass of Voyager 2 Kane et al. (1995) also report values of $\omega/\Omega_{\mathrm{J}} \approx 0.5$ at $\sim 70R_{\mathrm{J}}$, falling to $\sim$0.3 at $\sim 120R_{\mathrm{J}}$.

Overall, therefore, these observations are consistent with angular velocities which are close to corotation within ~ 10–$20R_{\mathrm{J}}$, then fall to $\omega/\Omega_{\mathrm{J}} \approx 0.5$ at $\sim 50R_{\mathrm{J}}$, and to even smaller values at larger distances (should the current sheet extend beyond that distance in a particular local time sector). Here we have therefore adopted the simple empirical form

$$\left(\frac{\omega}{\Omega_{\mathrm{J}}}\right) = \frac{1}{(1+(\rho_{\mathrm{e}}/\rho_{\mathrm{eo}})^{n})}, \tag{17}$$

where $\rho_{\mathrm{eo}} = 50R_{\mathrm{J}}$. Thus for all positive n we have $\omega/\Omega_{\mathrm{J}} \to 1$ as $\rho_{\mathrm{e}} \to 0$, $\omega/\Omega_{\mathrm{J}} = 0.5$ at $\rho_{\mathrm{e}} = \rho_{\mathrm{eo}} = 50R_{\mathrm{J}}$, and $\omega/\Omega_{\mathrm{J}} \to 0$ as $\rho_{\mathrm{e}} \to \infty$. However, as n increases, so does the sharpness of the decrease in the angular velocity about $\rho_{\mathrm{e}} = \rho_{\mathrm{eo}}$. This is shown in Fig. 2a, where we plot the model values of $\omega/\Omega_{\mathrm{J}}$ versus ρ_{e} in the range 0–$100R_{\mathrm{J}}$ (the region considered here). Profiles are shown for $n = 2, 4$, and 6. The profile for $n = 2$ has the weakest gradient, and may be considered the most likely in terms of the above observations. In addition, in this case we have $\omega/\Omega_{\mathrm{J}} \propto \rho_{\mathrm{e}}^{-2}$ at large distances, in conformity with the simple ideas discussed above based on conservation of angular momentum. However, it remains of interest to consider how the results depend on the form of the angular velocity profile, and so we will also show results derived for the larger n values.

The third topic concerns the magnetic field model employed to determine the profiles of F_{e} and $B_{z\mathrm{e}}$ in the equatorial plane. Here we find it important to the resulting values of the field-aligned currents to employ a magnetic model which adequately represents the radially inflated field of the middle magnetosphere current sheet. To this purpose, we have taken the equatorial field within a certain distance ρ_{e}^{*} to be given by the dipole field plus the field of the Connerney et al. (1981) current sheet model (the CAN model). That is, we take

$$B_{z\mathrm{e}}(\rho_{\mathrm{e}}) = -\frac{B_{\mathrm{J}}R_{\mathrm{J}}^{3}}{\rho_{\mathrm{e}}^{3}} + B_{\mathrm{CAN}_z}(\rho_{\mathrm{e}}), \tag{18}$$

where

$$B_{\mathrm{CAN}_z}(\rho_{\mathrm{e}}) = \frac{\mu_{\mathrm{o}} I_{\mathrm{o}}}{2} \times \left\{ \begin{array}{l} \log\left[\dfrac{\sqrt{\rho_{\mathrm{e}}^{2}+D^{2}}+D}{\sqrt{\rho_{\mathrm{e}}^{2}+D^{2}}-D}\right] + \dfrac{R_{\mathrm{o}}^{2}D}{2(\rho_{\mathrm{e}}^{2}+D^{2})^{3/2}} \\ -\log\left[\dfrac{\sqrt{R_{1}^{2}+D^{2}}+D}{\sqrt{R_{1}^{2}+D^{2}}-D}\right] - \dfrac{\rho_{\mathrm{e}}^{2}D}{2(R_{1}^{2}+D^{2})^{3/2}} \end{array} \right\}. \tag{19}$$

This approximate form for the CAN model field is that recently derived by Edwards et al. (2000), and is an accurate representation of the model to within better than $\sim$1% in the region of interest. The model itself was fit to Voyager and Pioneer flyby data, and is reported by Connerney et al. (1981) as being a reasonable approximation to observed fields out to $\sim 30R_{\mathrm{J}}$. The model parameters employed here are the Voyager 1/Pioneer 10 set derived by Connerney

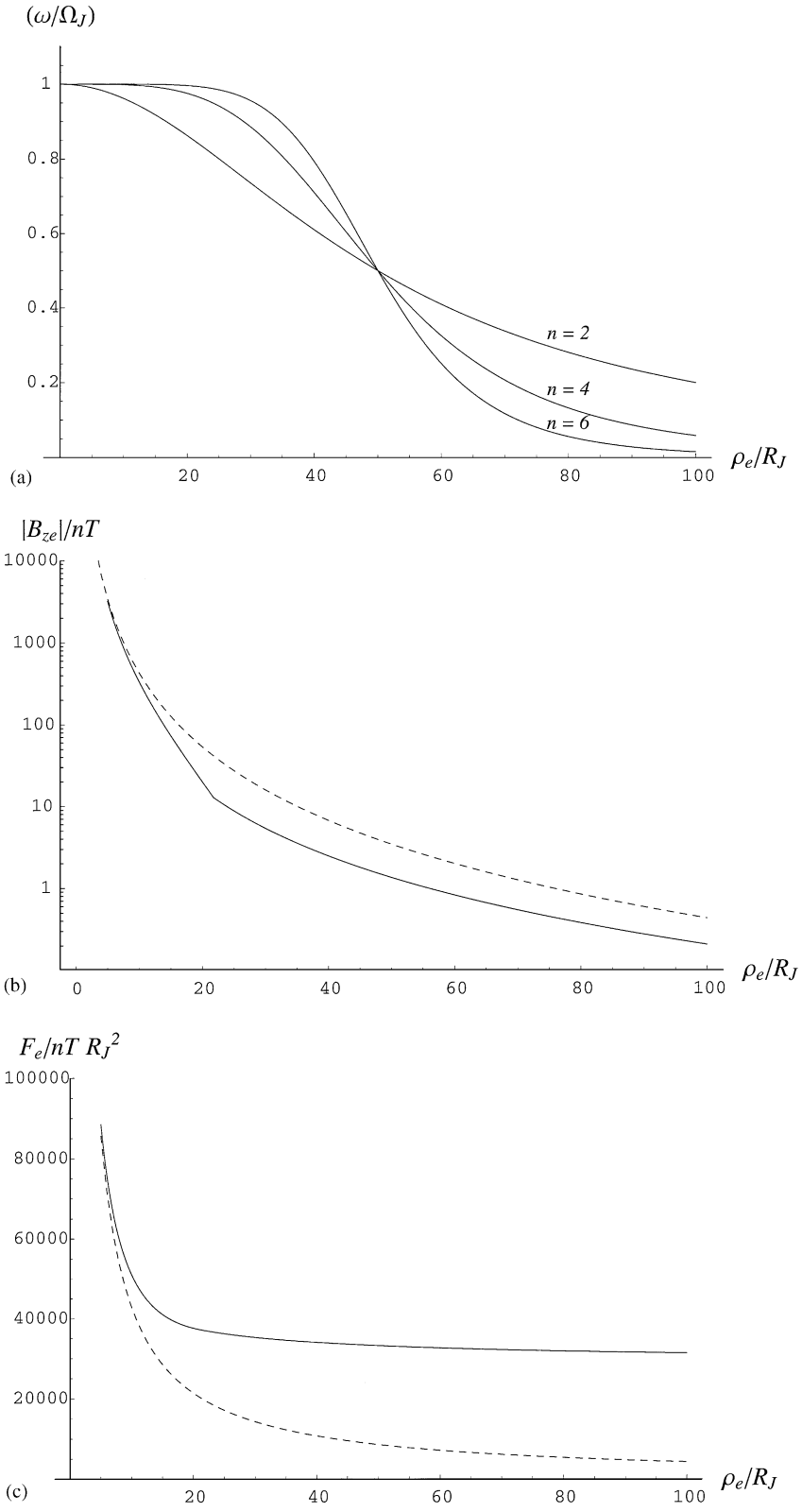

Fig. 2. Graphs of the parameters of our empirical model plotted versus equatorial jovicentric distance ρ_e. (a) Shows the angular velocity of the plasma in the equatorial plane normalised to the planetary angular velocity, (ω/Ω_J). (b) Shows a log-linear plot of the north–south equatorial field $|B_{ze}|$ threading the equatorial plane (solid line), where we note that the field is actually negative, i.e. points south. The kink at a distance of $21.78R_J$ marks the point where we switch from the dipole plus CAN model at small distances to the KK model at larger distances (see text). The dashed line shows the planetary dipole value. (c) Shows the equatorial flux function of the model magnetic field, F_e (solid line), compared with the planetary dipole value (dashed line).

et al. (1981), i.e. a current sheet half-thickness $D = 2.5R_J$, inner and outer radii of $R_o = 5R_J$ and $R_1 = 50R_J$, respectively, and a current intensity parameter $(\mu_o I_o/2) = 225$ nT. Beyond distance ρ_e^* we have employed the empirical B_{ze} model obtained from a fit to outbound Voyager 1 data by Khurana and Kivelson (1993), given by the power law

$$B_{ze}(\rho_e) = -A(R_J/\rho_e)^m, \tag{20}$$

where $A = 5.4 \times 10^4$ nT, and $m = 2.71$. For convenience we term this the KK model. This expression was obtained from a fit to data over the radial range ~20–100R_J, thus overlapping with the CAN model in the range ~20–30R_J. Here we have switched from one model to the other at the radial distance ρ_e^* where the two curves intersect, such that B_{ze} is continuous. For the models chosen, we find that this occurs at $\rho_e^* = 21.78R_J$, which thus lies within the region of overlap of their respective regimes of validity. The modulus of our model B_{ze} is plotted versus ρ_e in Fig. 2b (solid line) in log-linear format, together with the dipole value (dashed line) for purposes of comparison (the actual values of both are of course negative). The former is smaller than the latter typically by factors of ~2–3 in the middle magnetosphere region, due to the outward distension of the field lines in that region caused by the equatorial azimuthal currents.

With this model for B_{ze}, the flux function in the equatorial plane can now be determined. Within ρ_e^* we take the value corresponding to the planetary dipole plus the CAN model of the current sheet, given by

$$F_e(\rho_e) = \frac{B_J R_J^3}{\rho_e} + F_{e\,CAN}(\rho_e), \tag{21}$$

where

$$F_{e\,CAN}(\rho_e) = \frac{\mu_o I_o}{2} \times \left\{ \begin{array}{l} D\sqrt{\rho_e^2 + D^2} + \dfrac{\rho_e^2}{2}\log\left[\dfrac{\sqrt{\rho_e^2+D^2}+D}{\sqrt{\rho_e^2+D^2}-D}\right] - \dfrac{R_o^2 D}{2\sqrt{\rho_e^2+D^2}} - D^2 \\ -\dfrac{\rho_e^2}{2}\log\left[\dfrac{\sqrt{R_1^2+D^2}+D}{\sqrt{R_1^2+D^2}-D}\right] - \dfrac{\rho_e^4 D}{8(R_1^2+D^2)^{3/2}} \end{array} \right\}. \tag{22}$$

The expression for the flux function for the CAN model is again that presented by Edwards et al. (2000), which also represents the model function to better than ~1% in the region of interest. Beyond ρ_e^* we use Eq. (4) to find

$$F_e(\rho_e) = F_e(\rho_e^*) + \int_{\rho_e^*}^{\rho_e} d\rho_e'\, \rho_e' B_{ze}(\rho_e') = F_e(\rho_e^*) + \frac{AR_J^2}{(m-2)}\left[\left(\frac{R_J}{\rho_e}\right)^{m-2} - \left(\frac{R_J}{\rho_e^*}\right)^{m-2}\right], \tag{23}$$

where $F_e(\rho_e^*)$ is obtained from Eq. (21), and where we introduced Eq. (20) into the integral. The flux function obtained from Eqs. (21) and (23) is shown versus ρ_e by the solid line in Fig. 2c. The dashed line gives the corresponding dipole value. It can be seen that F_e exceeds the dipole value typically by factors of ~2–8, increasing with ρ_e, and still has a significantly large value of $\sim 3 \times 10^4$ nT R_J^2 at large ρ_e. Field lines with smaller values of F_e thus do not close within ~100R_J of the planet in this model, and can therefore be taken to correspond to the field lines of the distant tail, mostly to open flux in the tail lobes. We note that a value of $F \approx 3 \times 10^4$ nT R_J^2 corresponds to a dipole co-latitude of ~15° in the ionosphere (from Eq. (3)), which in turn corresponds to the region immediately poleward of the main auroral oval.

2.4. Field-aligned currents in the equatorial plane

We now use Eq. (14) and the above empirical model parameters to estimate the magnitude and form of the field-aligned currents which couple Jupiter's middle magnetosphere region to the ionosphere. Taking Σ_P^* to be constant, and performing the differentiation in Eq. (14) we have

$$\left(\frac{j_{||}}{B}\right) = 2\Sigma_P^*(\Omega_J - \omega) \times \left[\left(\frac{F_e}{\rho_e^2|B_{ze}|}\right)\left(\frac{1}{(\Omega_J-\omega)}\frac{d}{d\rho_e}(\Omega_J-\omega)\right) - 1\right], \tag{24}$$

and since from Eq. (17) we have

$$(\Omega_J - \omega) = \Omega_J \frac{(\rho_e/\rho_{eo})^n}{(1+(\rho_e/\rho_{eo})^n)}, \tag{25}$$

we then find

$$\left(\frac{j_{||}}{B}\right) = \frac{2\Sigma_P^*\Omega_J(\rho_e/\rho_{eo})^n}{(1+(\rho_e/\rho_{eo})^n)} \times \left[\left(\frac{F_e}{\rho_e^2|B_{ze}|}\right)\left(\frac{n}{1+(\rho_e/\rho_{eo})^n}\right) - 1\right], \tag{26}$$

where we have put $B_{ze} = -|B_{ze}|$ at Jupiter. We note that $(j_{||}/B)$ is positive (current flow from the ionosphere into the plasma sheet) where the first term in the bracket on the RHS exceeds the second, while the direction of current flow reverses in sense when the second term exceeds the first. It can be seen that, in addition to the exponent n describing the steepness of fall-off of the plasma angular velocity, the dimensionless parameter $(F_e/\rho_e^2|B_{ze}|)$ derived from the magnetic model is also crucial. For a dipole field this latter parameter is equal to unity, independent of distance. In Fig. 3a we show this parameter versus ρ_e for the empirical field model introduced above (the kink in the curve at $\rho_e^* = 21.78R_J$ occurs at the point where we switch from the dipole plus CAN model to the KK model). The value increases from near unity at small distances (where the planetary dipole is dominant) to ~15 at ~100R_J. This is due to the fact that for the model field the F_e value is higher than that of the dipole at a given distance, while $|B_{ze}|$ is smaller, as previously shown in Figs. 2b and c discussed above. Both combine to make the value of $(F_e/\rho_e^2|B_{ze}|)$ roughly an

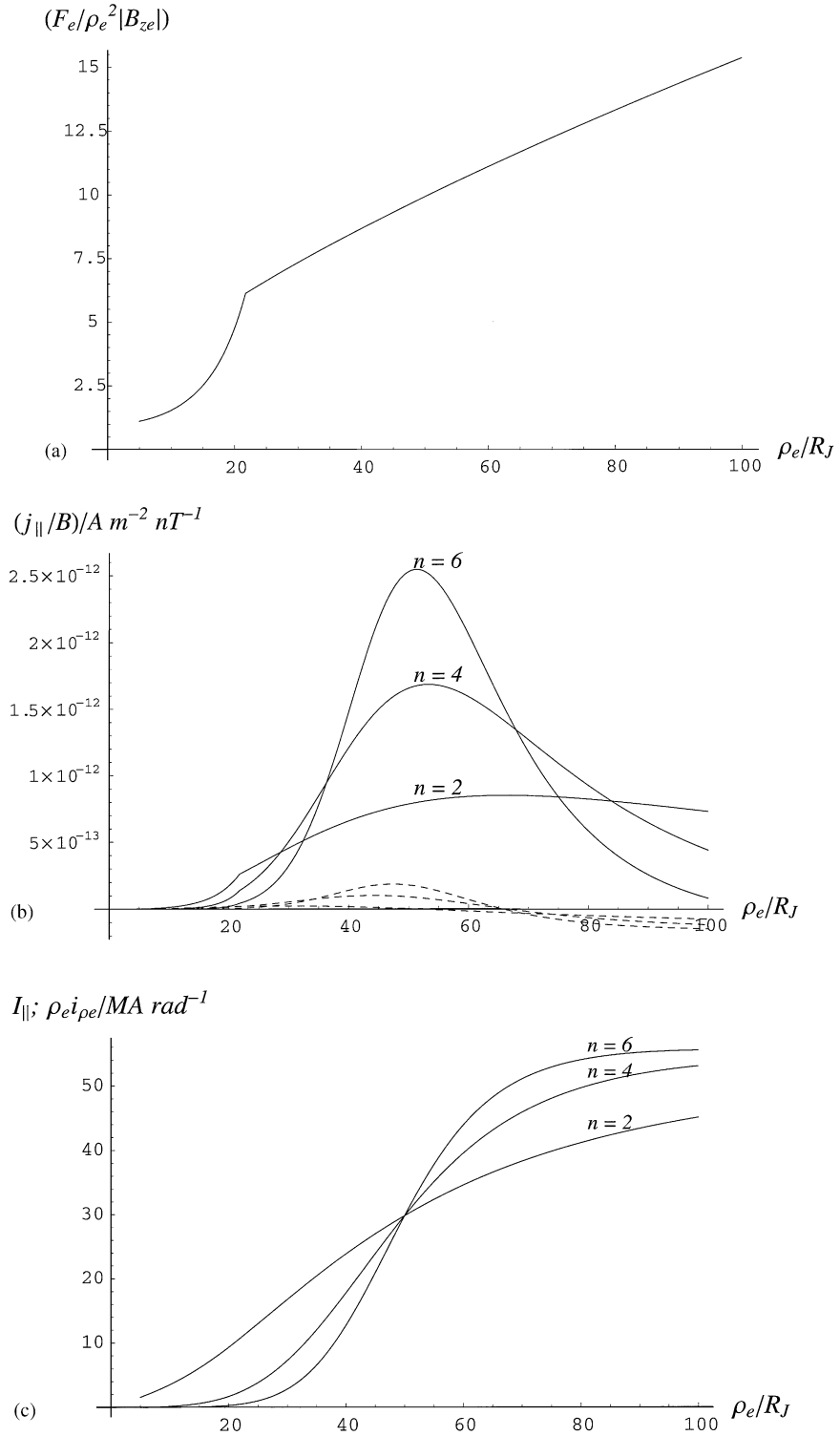

Fig. 3. (a) Shows the dimensionless parameter $(F_e/\rho_e^2|B_{ze}|)$ versus ρ_e for our empirical field model. For a dipole field this parameter is equal to unity for all ρ_e. (b) Shows $(j_{||}/B)$ versus ρ_e for our models with $n = 2, 4$, and 6 (solid lines). The dashed lines show the values derived using a dipole field for the same angular velocity profiles (shown for $n = 2, 4$, and 6 from the inner to the outer curves, respectively). (c) Shows the total radial current per radian of azimuth flowing in the current sheet, $\rho_e i_{\rho e}$, versus ρ_e, for $n = 2, 4$, and 6.

order of magnitude higher than the dipole value, and this is reflected in the model values of $(j_{||}/B)$ which we derive.

In Fig. 3b we therefore show the profiles of $(j_{||}/B)$ versus ρ_e derived from Eq. (26), using the model parameters described above. The dashed lines show values derived for a dipole field for $n = 2, 4$, and 6 (from the "inner" to the "outer" curves respectively). The values peak in $\sim$30–50R_J, depending on n, and then fall and reverse in

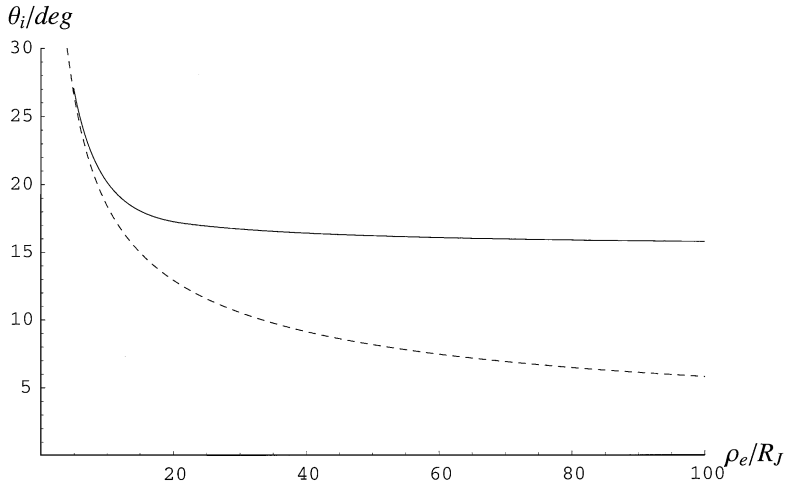

Fig. 4. Shows the mapping of the field lines between the equatorial plane and the ionosphere, given by the constancy of the flux function F along the field lines. The ionospheric co-latitude of the field lines θ_i is plotted versus equatorial radial distance ρ_e. The solid line shows the mapping for our empirical model, while the dashed line shows the planetary dipole mapping.

sense beyond $\sim$50–60R_J. Peak positive values are of order $\sim 10^{-13}$ A m^{-2} nT^{-1}, increasing with increasing n. The solid lines show values derived using the current sheet model field. Two major changes are observed. First, the current remains positive throughout the whole domain of interest, and does not reverse within $\sim 100R_J$. That is, for the simple but physically plausible model employed here, the sense of current flow into the plasma sheet is outwards from the ionosphere into plasma sheet throughout the whole of the middle magnetosphere region. This means that the "return" current flow will occur principally at the outer boundary of the middle magnetosphere region at large distances, rather than occurring in a more distributed way in the outer plasma sheet region, as discussed above in Section 2.2. Second, the magnitude of $(j_{||}/B)$ is increased by more than an order of magnitude, to values of order $\sim 10^{-12}$ A m^{-2} nT^{-1} beyond $\sim 30R_J$. For $n = 2$, the maximum value is 0.85×10^{-12} A m^{-2} nT^{-1} at $66R_J$, but the current is broadly distributed and slowly varying beyond $\sim 30R_J$. As n increases, the maximum values also increase, and become more sharply peaked near $\sim 50R_J$ where the angular velocity profile changes most rapidly. Maximum values are 1.68×10^{-12} A m^{-2} nT^{-1} at $53R_J$ for $n = 4$, and 2.54×10^{-12} A m^{-2} nT^{-1} at $51R_J$ for $n = 6$. We note that in a recent study, Bunce and Cowley (2001) have derived values of $(j_{||}/B)$ from analysis of magnetic field data obtained from several spacecraft flyby passes, in the radial range 20–50R_J. Values derived from analysis of the Voyager outbound passes, in particular, increase from $\sim 0.2 \times 10^{-12}$ A m^{-2} nT^{-1} at $\sim 20R_J$, to $\sim 1.0 \times 10^{-12}$ A m^{-2} nT^{-1} at $\sim 50R_J$, very much in the manner we have derived here for the current sheet field model. The values shown in Fig. 3b thus appear to be realistic in both form and amplitude, within present (albeit limited) knowledge. In the next section we map these currents into the ionosphere, using Eq. (15), and discuss the implications.

Here, however, we present in Fig. 3c the total integrated field-aligned current $I_{||}$ per radian of azimuth (both ionospheres combined) versus ρ_e, given by Eq. (16), for n=2, 4, and 6. This quantity is, of course, also equal to the total radial current per radian of azimuth flowing in the plasma sheet, $\rho_e i_{\rho e}$. This current grows from small values at small ρ_e to a value of $\sim$30 MA rad^{-1} at $50R_J$, equal for all models, and then to values of $\sim$45, $\sim$53, and $\sim$55 MA rad^{-1} at $100R_J$ for $n = 2$, 4, and 6, respectively. Each of the curves increase monotonically with ρ_e, in conformity with the consistent sense of $j_{||}$ shown in the middle panel. Integrated over azimuth, the total radial current at $\sim 100R_J$ is thus estimated to be $\sim$300 MA. The value deduced by Connerney (1981) from analysis of Pioneer 10 azimuthal field data was 140 MA, lower than this estimate by a factor of $\sim$2. These values compare with the total azimuthal current flowing in the current sheet in the same region of $\sim$300 MA. However, of this total, the majority of the azimuthal current, $\sim$180 MA, flows in the inner part of the system between $\sim$5 and $\sim 20R_J$ where the radial current is relatively small.

3. Ionospheric currents and field-aligned voltages

3.1. Ionospheric field-aligned currents

In this section we now map the field-aligned currents derived in the previous section down into the ionosphere using the constancy of $(j_{||}/B)$ and Eq. (15). As indicated above, the mapping is achieved using the constancy of the flux function F along the field lines. From Eq. (3) we thus find that the ionospheric co-latitude θ_i of a field line which passes through the equator at a radial distance ρ_e is given by

$$\sin^2 \theta_i = \left(\frac{F_e(\rho_e)}{B_J R_J^2} \right), \tag{27}$$

where $F_e(\rho_e)$ is given by Eqs. (21) and (23). This mapping is shown by the solid line in Fig. 4, where we plot θ_i versus ρ_e.

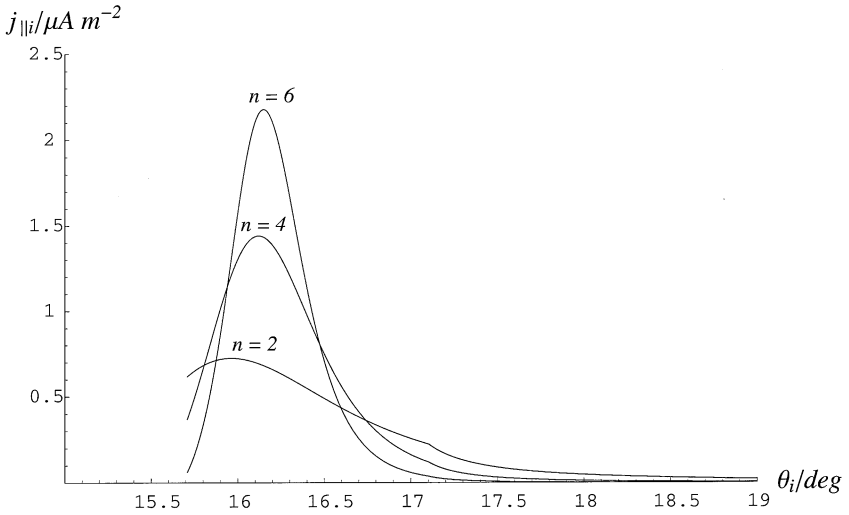

Fig. 5. Profiles of the upward ionospheric field-aligned current $j_{||i}$ plotted versus co-latitude θ_i, for the flow models with $n = 2, 4$, and 6. The curves terminate at small co-latitudes at the field line that maps to the outer limit of our model at $100R_J$ in the equatorial plane. The field line at 19° co-latitude at the right-hand border maps to $12.1R_J$ in the equatorial plane, such that the whole mapping of the middle magnetosphere into the ionosphere is covered by this plot.

The dashed line shows the dipole mapping for purposes of comparison. Unlike the dipole mapping, which falls to small values of θ_i (close to the magnetic pole) for large $\rho_e \sim 100R_J$, the current sheet field mapping asymptotes to values of θ_i just above $\sim 15^\circ$ at such ρ_e values, as noted above. The field lines at higher latitudes thus, in the main, represent tail field lines, as previously noted. Furthermore, we also note the extremely narrow range of latitudes into which the middle magnetosphere current sheet maps in the ionosphere. The whole of the equatorial region between $\sim 20R_J$ and $\sim 100R_J$ maps into a latitudinal strip little more than $\sim 1^\circ$ wide. At Jupiter, 1° of latitude corresponds to a horizontal north–south distance of ~ 1250 km.

Using this mapping and Eq. (15), we present in Fig. 5 the profiles of upward ionospheric field-aligned current, $j_{||i}$, versus co-latitude θ_i for $n = 2, 4$, and 6. It can be seen that in each case the main part of the field-aligned current maps into a region $\sim 1^\circ$ wide, centred at a co-latitude of $\sim 16^\circ$, in conformity with the above discussion. These values correspond very well to those of the main auroral oval, as mentioned in the introduction. With increasing values of the plasma angular velocity exponent n, the width of the current-carrying region narrows somewhat, and the peak current increases. Maximum values are 0.72 μA m^{-2} for $n = 2$, 1.44 μA m^{-2} for $n = 4$, and 2.18 μA m^{-2} for $n = 6$. Thus while the details of the current distribution depend on the form of the angular velocity profile, as expected, the basic values of the current parameters do not. Upward-directed ionospheric field-aligned currents mapping to the middle magnetosphere are estimated to be of amplitude ~ 1 μA m^{-2}, restricted to a latitudinal region of width ~ 1000 km. We note that such current densities are also entirely typical of the large-scale ionospheric field-aligned currents which couple the magnetosphere–ionosphere system in the Earth's environment (e.g. Iijima and Potemra, 1978).

3.2. Field-aligned voltages and precipitating electron energy fluxes

We now consider the conditions required for the ionospheric field-aligned currents derived above to flow. For a current to flow from the ionosphere to the magnetosphere we require either that ions flow out from the ionosphere to the magnetosphere, or that electrons flow in from the magnetosphere to the ionosphere, or some combination of the two. However, as in the case of the Earth, it seems very unlikely that ionospheric ions can provide the required current at Jupiter. If we assume, for example, that the ion flux at high altitudes is limited to values estimated for the polar wind outflow, then typical net outflow fluxes at ionospheric heights are likely limited to $\sim 10^{11}$ m^{-2} s^{-1} (Swartz et al., 1975), or perhaps $\sim 10^{12}$ m^{-2} s^{-1} in the most favourable circumstances (Nagy et al., 1986). These fluxes correspond to current densities of ~ 0.01–0.1 μA m^{-2}, which even in the more favourable circumstance is less than the required current density by about an order of magnitude. We therefore assume that the upward currents will be carried principally by downward-precipitating magnetospheric electrons, and for simplicity we will henceforth neglect the ionospheric ion contribution.

In the case of the Earth, it is found that field-aligned voltages of order a few kV are required to drive upward field-aligned currents at densities which are comparable

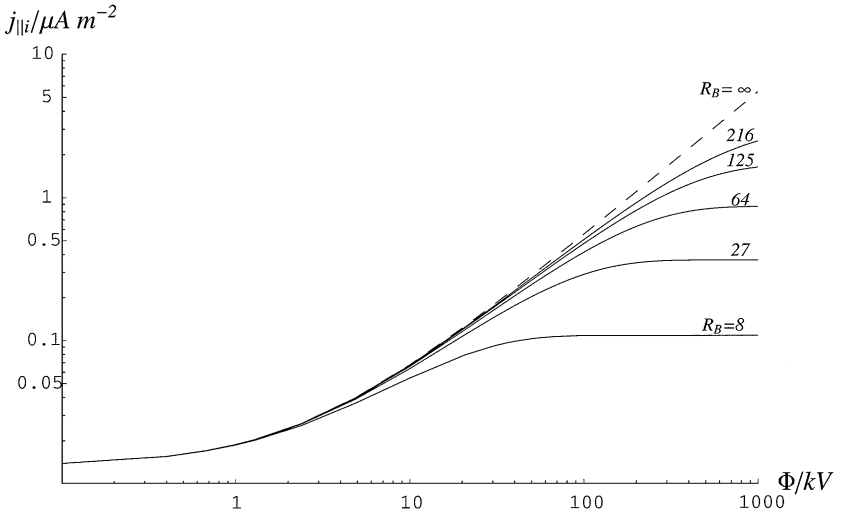

Fig. 6. Log–log plot of the Knight relation between the ionospheric field-aligned current density, $j_{||i}$, and the field-aligned voltage, Φ, for various values of the ratio R_B of the magnetic field strength B_i in the ionosphere and the field strength B_Φ at the "top" of the acceleration region. Results are shown specifically for an isotropic Maxwellian magnetospheric population with a density $N = 0.01$ cm^{-3}, and a thermal energy $W_{th} = 2.5$ keV. The solid lines are for $R_B = 8$, 27, 64, 125, and 216, corresponding to jovicentric distances of the "top" of the acceleration region of approximately $2R_J, 3R_J, 4R_J, 5R_J$, and $6R_J$, respectively. The dashed line shows the limiting case for $R_B = \infty$.

with those estimated here. In the absence of a field-aligned voltage, the maximum field-aligned current which can be carried by precipitating magnetospheric electrons at ionospheric heights is given by

$$j_{||i}(0) = eN\left(\frac{W_{th}}{2\pi m_e}\right)^{1/2}, \tag{28}$$

where e is the elementary charge, m_e the mass of an electron, N the magnetospheric electron number density, and W_{th} the thermal energy. Eq. (28) corresponds to having a full downward-going loss cone at the top of the ionosphere, and an empty upward-going loss cone. Now in assessing the magnitude of $j_{||i}(0)$ at Jupiter, it is important to emphasise that the magnetospheric plasma electrons which carry the current do not correspond to those of the cool relatively dense plasma in the plasma sheet, which are electrostatically confined to the equatorial region occupied by the outwardly diffusing heavy iogenic ions. Rather, they correspond to the hotter more tenuous plasma population which extends outside of the plasma sheet down to the ionosphere. Scudder et al. (1981) have studied this population in some detail using Voyager thermal electron data, and indicate that typical number densities are $\sim$0.01 cm^{-3}, while typical thermal energies are $\sim$2.5 keV. These are the values we have adopted here. Using them in Eq. (28) we find that $j_{||i}(0) \approx 0.013$ μA m^{-2}, which is less than the values we have derived above by factors of 50–100. It therefore seems inescapable that large field-aligned voltages are required to carry the field-aligned currents we have estimated.

The relationship between the field-aligned current carried by precipitating electrons and the field-aligned voltage was first derived by Knight (1973), and is given by

$$j_{||i}(\Phi, R_B) = j_{||i}(0)R_B \times\left[1-\left(1-\frac{1}{R_B}\right)\exp\left(-\frac{e\Phi}{W_{th}(R_B-1)}\right)\right], \tag{29}$$

where $j_{||i}(0)$ is as in Eq. (28), Φ is the field-aligned voltage, and $R_B = (B_i/B_\Phi)$ is the ratio of the magnetic field strength in the ionosphere, B_i, and the field strength at the top of the voltage drop, B_Φ. The expression assumes an isotropic Maxwellian velocity distribution in the magnetosphere (such that N is independent of distance along the field lines in the absence of loss cones), though subsequent work has shown that the results are not very sensitive to other reasonable assumptions concerning the energy distribution (Pierrard, 1996; Dors and Kletzing, 1999). The result is also independent of the distribution of the field-aligned voltage along the field lines, under the simplifying assumption that no particles mirror before experiencing the full voltage. We note that considerable work over the past twenty years has established in some detail the applicability of Eq. (29) in the terrestrial environment (e.g. Lyons et al., 1979; Bosqued et al., 1986; Weimer et al., 1987; Shiokawa et al., 1990, 2000; Lu et al., 1991; Haerendel et al., 1994; Olsson et al., 1996; Stauning, 1998; Antonova et al., 1999). Here we now apply it to Jupiter.

In Fig. 6 we show in log–log format the current voltage relationship given by Eqs. (28) and (29) for various values of R_B, specifically for $N = 0.01$ cm^{-3}, and $W_{th} = 2.5$ keV. The curves shown by the solid lines are for $R_B = 8, 27, 64, 125$, and 216, corresponding to cases in which the top of the acceleration region is located at jovicentric distances of approximately $2R_J, 3R_J, 4R_J, 5R_J$, and $6R_J$, respectively (for a dipole field which falls off as the inverse cube of the

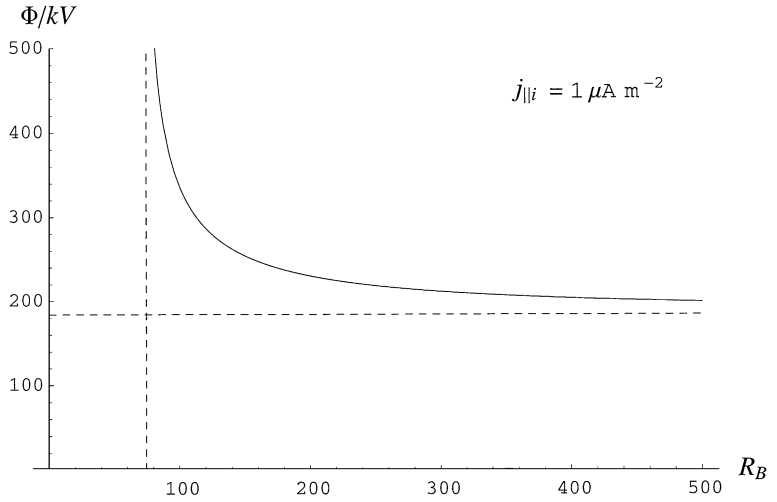

Fig. 7. Plot of the field-aligned voltage Φ versus R_B given by Eq. (33) for an ionospheric current of $j_{||i} = 1$ μA m^{-2} and a magnetospheric population with $N = 0.01$ cm^{-3} and $W_{th} = 2.5$ keV, such that the maximum ionospheric field-aligned current without a field-aligned voltage is $j_{||i}(0) = 0.013$ μA m^{-2}. The minimum value of R_B for which there is a solution, 74.6, is marked by the dashed vertical line. Above this value of R_B the voltage falls rapidly towards the minimum value of 184 kV, marked by the dashed horizontal line.

distance). The dashed line shows the limiting case $R_B \to \infty$, such that taking the argument in the exponent in Eq. (29) to be small, we find

$$j_{||i_{max}}(\Phi) = j_{||i}(\Phi, R_B \to \infty) = j_{||i}(0)\left(1 + \left(\frac{e\Phi}{W_{th}}\right)\right), \quad (30)$$

i.e. a linear relationship between the current and the voltage. We have termed this quantity $j_{||i_{max}}(\Phi)$ because it is the maximum ionospheric current density that can be obtained for a given voltage for given magnetospheric conditions. It can be seen that for small values of the voltage the current is equal to $j_{||i}(0)$ independent of Φ and R_B, and only starts to increase significantly above this value when $e\Phi$ increases above $\sim W_{th}$. The curves then increase, following closely the $R_B \to \infty$ approximation given by Eq. (30), until $e\Phi$ increases above $\sim R_B W_{th}$. Above this voltage, the current saturates at the value

$$j_{||i}(\Phi \to \infty, R_B) = R_B j_{||i}(0). \quad (31)$$

The saturation current corresponds to the situation in which all the electrons which reach the "top" of the acceleration region (where $B = B_\Phi = B_i/R_B$) are accelerated along the field into the ionosphere and contribute to the current. The convergence of the field lines then amplifies the precipitating electron flux at the ionosphere (and hence the current) by the factor $R_B = (B_i/B_\Phi)$ compared with the case where the voltage is zero.

Using these curves we can now consider the conditions required such that a certain current density $j_{||i}$ will flow at ionospheric heights. If $j_{||i} \geqslant j_{||i}(0)$, as shown above, then a voltage Φ must exist along the field lines, the minimum value of which is given by the $R_B \to \infty$ solution given by Eq. (31), i.e.

$$e\Phi_{min} = W_{th}\left(\left(\frac{j_{||i}}{j_{||i}(0)}\right) - 1\right). \quad (32)$$

We estimated above that the current densities required at Jupiter are about two orders of magnitude higher than $j_{||i}(0)$. The voltages required, and the resulting particle accelerations, are therefore also very large, of order $\sim 100 W_{th}$. That is, the auroral electrons must be accelerated to energies two orders of magnitude higher than magnetospheric energies. Since W_{th} is of order ~ 1 keV, the implied voltages are of order ~ 100 kV, and the electrons are accelerated to ~ 100 keV (near the upper limit for non-relativistic theory). For a finite value of R_B, the voltage is higher than that given by Eq. (32), and instead Eq. (29) gives

$$e\Phi = (R_B - 1) W_{th} \log\left[\frac{R_B - 1}{R_B - (j_{||i}/j_{||i(0)})}\right]. \quad (33)$$

As is evident from Fig. 6, the required voltage is infinite when $R_B = (j_{||i}/j_{||i}(0))$, and then falls as R_B increases towards Φ_{min} given by Eq. (32). No solutions exist for R_B less than $(j_{||i}/j_{||i}(0))$. In Fig. 7 we show an example for a magnetospheric population with the same parameters as chosen above (i.e. $N = 0.01$ cm^{-3} and $W_{th} = 2.5$ keV) such that $j_{||i}(0) = 0.013$ μA m^{-2}, where we plot Φ versus R_B for a typical required ionospheric current of $j_{||i} = 1$ μA m^{-2}. The minimum value of R_B, for which the required voltage is infinite, is $R_B = 74.6$ in this case (corresponding to a jovicentric distance of $4.2 R_J$ as discussed further below), marked by the dashed vertical line. Above this value of R_B the voltage falls rapidly with increasing R_B towards the minimum value of 184 kV given by Eq. (32), marked by the dashed horizontal line. Thus the "top" of the acceleration region does not have to lie at great distances above the minimum value, given by the minimum R_B value, before the required voltage falls to values close to the minimum value. For example, suppose the top of the voltage drop lies at a jovicentric distance of $6 R_J$ (compared with the minimum distance of $4.2 R_J$), such

that $R_B = 216$. Then the required voltage is 225 kV compared with the minimum value of 184 kV. Here we will therefore take the minimum voltage given by Eq. (32) as a sufficient approximation for the present estimates.

It is also of interest to consider the minimum distance of the "top" of the acceleration region, given by the minimum value of R_B for which there exists a solution for a given $j_{||\mathrm{i}}$. From Eq. (31) the minimum value of R_B is given by

$$R_{B_{\min}} = \left(\frac{B_\mathrm{i}}{B_{\Phi_{\max}}}\right) = \left(\frac{j_{||\mathrm{i}}}{j_{||\mathrm{i}}(0)}\right). \tag{34}$$

For the polar dipole field we have

$$\left(\frac{B_\mathrm{i}}{B_\Phi}\right) \approx \left(\frac{r}{R_\mathrm{J}}\right)^3, \tag{35}$$

where r is the jovicentric radial distance. Thus the "top" of the voltage drop must extend to a jovicentric distance of at least $r_{\min}$ given by

$$\left(\frac{r_{\min}}{R_\mathrm{J}}\right) \approx \left(\frac{j_{||\mathrm{i}}}{j_{||\mathrm{i}}(0)}\right)^{1/3}. \tag{36}$$

Noting again that we require currents about two orders of magnitude higher than $j_{||\mathrm{i}}(0)$, we thus typically require the acceleration region to extend to jovicentric distances above $\sim 4R_\mathrm{J}$.

In Fig. 8a we thus show the minimum voltage $\Phi_{\min}$ along the jovian polar field lines given by Eq. (32), plotted versus the ionospheric co-latitude θ_i for our empirical models with $n = 2, 4$, and 6. Apart from the small offset value of $(W_{\mathrm{th}}/e) = 2.5$ kV on the RHS of Eq. (32), essentially negligible in the present context, the value of Φ scales with the value of $j_{||\mathrm{i}}$ shown previously in Fig. 5. As for the ionospheric current, therefore, significant values of the voltage thus extend over latitudinal distances of $\sim 1^\circ$, centred near $\sim 16^\circ$, with peak values of 133, 266, and 404 kV for $n = 2, 4$, and 6, respectively. We note, however, that since these values scale, very nearly, with the current, they also scale with the value of the effective ionospheric Pedersen conductivity Σ_P^*, which we have assumed to be 0.5 mho. For smaller or larger values of Σ_P^*, so the voltages will be smaller or larger in proportion. However, for reasonable values in the range, say, $\sim$0.2–1 mho, the voltages will typically be in the range $\sim$50–250 kV for slowly varying angular velocity profiles such as the $n = 2$ model.

The magnetosphere–ionosphere coupling circuit will therefore typically accelerate electrons to high energies $\sim$50–250 keV along the field lines down into the ionosphere. Such energies are consistent with the low altitudes at which both visible and UV auroras are observed to occur (e.g. Prangé et al., 1998; Vasavada et al., 1999), as noted above. The observed UV auroral spectrum also requires the presence of high-energy electrons above $\sim$50 keV (Ajello et al., 1998), though also indicating the presence of a broad spectrum, rather than the essentially mono-energetic beam that would be produced by the present mechanism. However, as at Earth, we expect that a secondary population of electrons will form via scattering processes underneath the acceleration region, with energies extending in a relatively flat spectrum between low energies and the beam energy (Evans, 1974). These particles will be trapped between low-altitude magnetic mirror points and high-altitude electrostatic reflection points, while being diffused and precipitated by plasma waves.

In Fig. 8b we similarly show the minimum jovicentric radial distance of the top of the acceleration region, given by Eq. (36), plotted versus ionospheric co-latitude. Values are typically in the range $\sim 3R_\mathrm{J}$ to $\sim 5R_\mathrm{J}$ over the main part of the current-carrying region. We note that these distances scale as the cube root of the field-aligned current density, hence as the cube root of the assumed value of the effective ionospheric Pedersen conductivity. These results do not, therefore, vary greatly with the conductivity value assumed, over the range of reasonable values. The implication of these results is that accelerated field-aligned electron beams will be present over a broad range of jovicentric distances away from Jupiter, extending to at least ~ 4–$5R_\mathrm{J}$. We assume that these electrons provide a major source of free energy for jovian radio emissions. If the radio waves are produced at a frequency close to the local electron cyclotron frequency, e.g. via the cyclotron maser instability as is commonly assumed for both Earth and the outer planets (e.g. Ladreiter et al., 1994; Zarka, 1998), then the implication is for a broad-band source extending from frequencies of $\sim$100 kHz at the "top" of the acceleration region to $\sim$20 MHz at the auroral ionosphere. Such frequencies correspond essentially to the jovian b-KOM, HOM and non-Io-DAM radio emissions (e.g. Zarka, 1998). We suggest that the mechanism discussed here provides not only an explanation for the main auroral oval at Jupiter, but also for a major component of its radio emissions. In Section 4 we discuss the implications for the expected solar wind modulation of both the auroral and the radio emissions.

We now consider the precipitated energy flux of the auroral electrons, and the consequent auroral brightness. Without field-aligned acceleration, the maximum energy flux of the magnetospheric electrons into the ionosphere is given by

$$E_\mathrm{f}(0) = 2NW_{\mathrm{th}}\left(\frac{W_{\mathrm{th}}}{2\pi m_\mathrm{e}}\right)^{1/2}, \tag{37}$$

which is essentially the unaccelerated current density per elementary charge given by Eq. (28) (i.e. the unaccelerated number flux) times a characteristic energy. This is also the maximum energy flux that can be delivered to the ionosphere by magnetospheric pitch angle diffusion in the strong diffusion limit. For the magnetospheric parameters employed above, i.e. $N = 0.01$ cm^{-3} and $W_{\mathrm{th}} = 2.5$ keV, we find $E_\mathrm{f}(0) \approx 0.07$ mW m^{-2}. Assuming that this is converted with 20% efficiency into UV auroral photons of energy 10 eV, the brightness of the resulting aurora will be $\sim$0.8 kR. These values compare with the main oval energy fluxes of $\sim$10–200 mW m^{-2} and corresponding

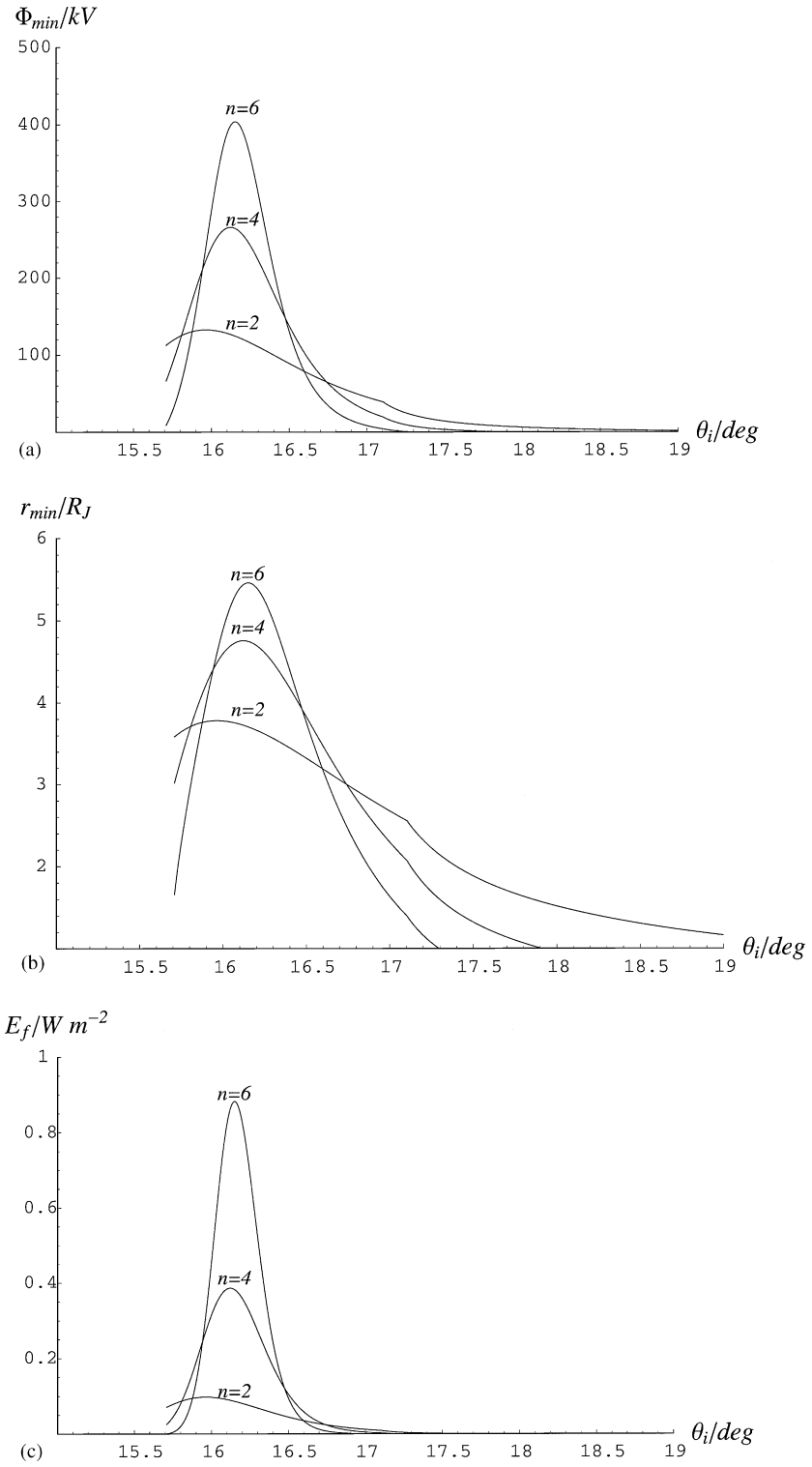

Fig. 8. (a) Shows the minimum field-aligned voltage $\Phi_{\min}$ required to drive the field-aligned current plotted versus ionospheric co-latitude θ_i, derived from Eq. (32) for our empirical models with $n = 2, 4$, and 6. (b) Shows the minimum jovicentric distance of the "top" of the acceleration region along the auroral field lines, $r_{\min}$, given by Eq. (36). (c) Shows the precipitated energy flux in the $R_B \rightarrow \infty$ approximation given by Eq. (39).

auroral brightnesses of ~100 kR to ~2 MR estimated from Hubble Space Telescope observations by Prangé et al. (1998). Thus as discussed in the introduction, without acceleration, energy fluxes are two orders of magnitude lower than those required to explain even the lowest intensities observed in the main oval, even in the strong diffusion (full loss-cone) limit. However, field-aligned auroral acceleration increases the precipitated energy flux through two effects.

The first is that the electron number flux reaching the ionosphere is enhanced by the field-aligned collimation of the field-aligned accelerated particles. The value of the number flux is set by the required field-aligned current density, such that the enhancement factor required is $(j_{||i}/j_{||i}(0))$, which is around ~50–100 as noted above. The second factor is that the typical energy of the auroral electrons is enhanced by the voltage drop, which involves essentially the same factor, as indicated by Eq. (32) above. The energy flux is thus enhanced by a factor of order $(j_{||i}/j_{||i}(0))^2$, i.e. a factor of about 10^3–10^4. Thus the energy flux we obtain is of order ~0.1–1 W m^{-2}, corresponding to a 1–10 MR aurora. The mechanism is thus able to account for the brightest of main oval emissions.

In more detail, under the same assumptions that led to Eq. (29) for the current density, Lundin and Sandahl (1978) showed that the precipitated energy flux of the accelerated electrons is given by

$$E_f(\Phi, R_B) = \frac{1}{2} E_f(0) R_B \left[\left(2 + \frac{e\Phi}{W_{th}}\right) - \left(\frac{e\Phi}{W_{th}} + 2\left(1 - \frac{1}{R_B}\right)\right) \exp\left(-\frac{e\Phi}{W_{th}(R_B - 1)}\right)\right], \tag{38}$$

where $E_f(0)$ is given by Eq. (37), and we have used the same notation as above. Here we will take the limit $R_B \to \infty$ to a sufficient approximation, equivalent to the minimum accelerating voltage given by Eq. (32). In this limit we then have

$$E_f(\Phi, R_B \to \infty) = E_f(0)\left[1 + \left(\frac{e\Phi_{min}}{W_{th}}\right) + \frac{1}{2}\left(\frac{e\Phi_{min}}{W_{th}}\right)^2\right], \tag{39}$$

where we see that $E_f(0)$ is enhanced by a factor which is in accord with the above discussion (the leading term being the last one in the bracket on the RHS).

In Fig. 8c we thus show the precipitated auroral electron energy flux versus ionospheric co-latitude, calculated from Eq. (39) for our empirical models with $n = 2, 4$, and 6. Peak values are 0.10, 0.39, and 0.88 W m^{-2} for $n = 2, 4$, and 6, respectively. According to the above discussion, these energy fluxes correspond to a peak UV auroral brightness of ~1, ~4, and ~9 MR respectively. These model values scale approximately as the square of the assumed value of the effective ionospheric Pedersen conductivity, and thus may be considered uncertain by a factor of at least ~4 in either direction. The latitudinal extent of the model emission (FWHM) is ~940, ~600, and ~410 km, respectively. These values thus provide a reasonable explanation of the principal characteristics of the main jovian auroral oval, as discussed in the introduction.

3.3. Magnetospheric and ionospheric potentials

The results derived above have shown that in order for the field-aligned currents to flow which are required by the magnetosphere–ionosphere coupling circuit, large field-aligned voltages ~100 kV must exist along the auroral field lines. That is, the feet of the auroral field lines in the ionosphere must be at a higher positive potential by ~100 kV than on the same field lines in the equatorial plane. These are very large potential differences, and in this section we finally examine the implications for the structure of the potential in the ionosphere. In fact we will show that because the magnetospheric voltages are so large, only a modest rearrangement of the equipotentials are involved from an electrostatic viewpoint.

We begin by calculating the electrostatic potential in the equatorial plane which is associated with our empirical model. This is obtained by integrating the radial electric field associated with the equatorial flow, given by

$$E_r(\rho_e) = -V_\varphi(\rho_e) B_z(\rho_e) = -\rho_e \omega(\rho_e) B_z(\rho_e), \tag{40}$$

where $\omega(\rho_e)$ is given by Eq. (17), and $B_z(\rho_e)$ by Eqs. (18) and (20). Taking the arbitrary zero of potential to be at the outer limit of our model at a radial distance of $100R_J$ in the equatorial plane, we then have the equatorial potential $\Phi_e(\rho_e)$ given by

$$\Phi_e(\rho_e) = \int_{\rho_e}^{100R_J} E_r(\rho'_e)\, d\rho'_e = -\int_{\rho_e}^{100R_J} \rho'_e \omega(\rho'_e) B_z(\rho'_e)\, d\rho'_e, \tag{41}$$

where we note that since B_z is negative in the equatorial plane, potential Φ_e takes positive values. We have numerically integrated this formula, and in Fig. 9 show Φ_e versus ρ_e for our models with $n = 2, 4$, and 6, in log-linear format. The total voltage between the inner edge of the model current sheet at $\rho_e = 5R_J$ and the outer edge of the model at $100R_J$ is ~50 MV, and thus much larger than the field-aligned voltages required here. However, the voltage across the middle magnetosphere region where the field-aligned voltages actually occur (and hence across the main auroral oval ionosphere), say between $\sim 25R_J$ and $100R_J$, is much smaller, ~2.5 MV, and is thus only a factor of ten larger than the field-aligned voltages themselves. A more careful study is therefore warranted.

We have thus mapped the equatorial voltages along the field lines into the ionosphere assuming equipotentiality of the field lines, and have then examined how the ionospheric potential structure is changed when the field-aligned potentials are added. In Fig. 10 we show results for n=2, 4, and 6 in panels (a), (b), and (c), respectively. The short-dashed lines show the potential versus ionospheric co-latitude assuming the field lines are electric equipotentials. The field-aligned potential is then shown by the long-dashed lines, as shown previously in Fig. 8a. The total ionospheric potential Φ_i is the sum of these two, and is shown by the solid lines. It can be seen that the total potential remains monotonically varying in each case, and differs relatively little from the values deduced from assuming that the field lines are equipotentials. From an electrostatic viewpoint, therefore,

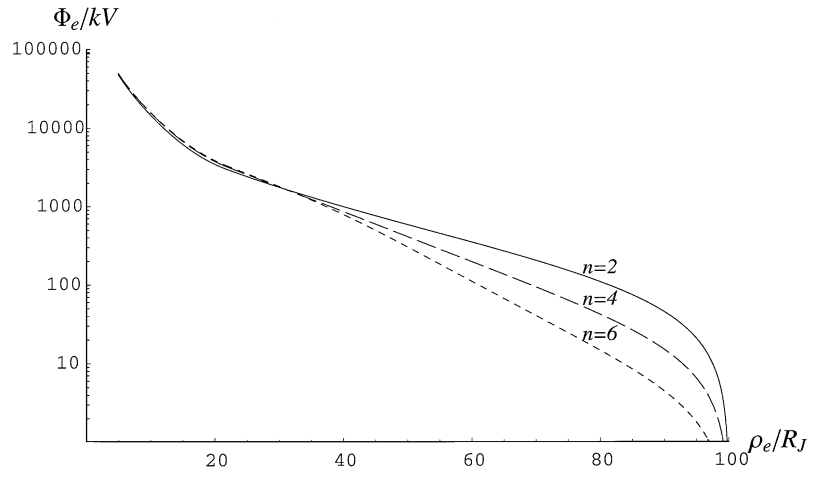

Fig. 9. Log-linear plot showing the electrostatic potential in the equatorial plane, Φ_e, versus equatorial jovicentric distance ρ_e, obtained by numerical integration of Eq. (41). Results are shown for $n = 2$ (solid line), $n = 4$ (long-dashed line), and $n = 6$ (short-dashed line). In each case the arbitrary zero of potential has been chosen to lie at the outer limit of our model at $100R_J$.

the field-aligned voltages can be produced by relatively small poleward displacements of the equipotentials across the field lines, through distances of order $\sim 0.1^\circ$–0.2° (100–200 km) at ionospheric heights.

At the same time, however, we note that the field-aligned potentials result in a lack of complete self-consistency in our model, since their existence modifies the field-perpendicular electric field in the ionosphere, and hence the Pedersen current from which we calculated the field-aligned currents. In a self-consistent solution, the Pedersen current should be calculated from the total field-perpendicular electric field in the ionosphere, given by the field mapped from the magnetosphere modified by the effect of the field-aligned potential. We note from Fig. 10 that the perturbing ionospheric electric fields are relatively small for the $n = 2$ model, where they act to reduce the perpendicular electric field and current over most of the region of interest. However, the effect becomes much more important as the field-aligned voltages become larger with increasing n, strengthening the electric field in the poleward-most region and weakening it further equatorward (and thus tending to narrow the latitudinal extent of the largest field-aligned current and aurora). This effect should clearly be taken into account in future work. However, given the simplicity of our calculations this refinement is hardly warranted here, particularly considering the additional lack of self-consistency in not having included the modification of the ionospheric conductivity produced by the electron precipitation. While our study should generally give the right order of the effects expected, the details will undoubtedly become modified in more complex self-consistent calculations.

4. Summary and discussion

In this paper we have investigated the suggestion that the main jovian auroral oval is connected with the magnetosphere–ionosphere coupling current system associated with the breakdown of rigid corotation in the middle magnetosphere region. We have first employed a simple model of the magnetic field and plasma flow in the inner and middle magnetosphere, based on observations (albeit limited in the case of the flow), to estimate the magnitude and form of the field-aligned currents associated with the coupling current system. Although the details depend upon the precise flow model employed, we find for the simple models employed here that the currents are directed out of the ionosphere into the current sheet throughout the whole of the middle magnetosphere region, out to $\sim 100R_J$. Characteristic magnitudes are $(j_{||}/B) \approx 10^{-12}$ A m^{-2} nT^{-1} on field lines mapping beyond $\sim 25R_J$ in the equatorial plane. The return current to the ionosphere must then flow in the region which bounds the middle magnetosphere at its outer limit (e.g. the magnetopause region if the current sheet extends that far). Mapped to the ionosphere, these currents form circumpolar rings of upward field-aligned current which are located at $\sim 16^\circ$ magnetic co-latitude (according to our simple axisymmetric magnetic model), with a latitudinal width of only 0.5°–1° (i.e. $\sim$500–1000 km). The location and width are consistent with those of the main jovian auroral oval (Satoh et al., 1996; Prangé et al., 1998; Clarke et al., 1998; Vasavada et al., 1999). Peak magnitudes of the field-aligned current at ionospheric heights are estimated to be of order ~ 1 μA m^{-2}.

We then considered the conditions required to drive these currents via precipitating auroral electrons. Using typical parameters for the hot magnetospheric electrons outside the equatorial plasma sheet (a density of ~ 0.01 cm^{-3} and a temperature of 2.5 keV), based on Voyager observations, we find using Knight's (1973) theory that substantial field-aligned voltages are required to provide the necessary number flux to the ionosphere, of order ~ 100 kV. Furthermore, the acceleration region must extend to high altitudes

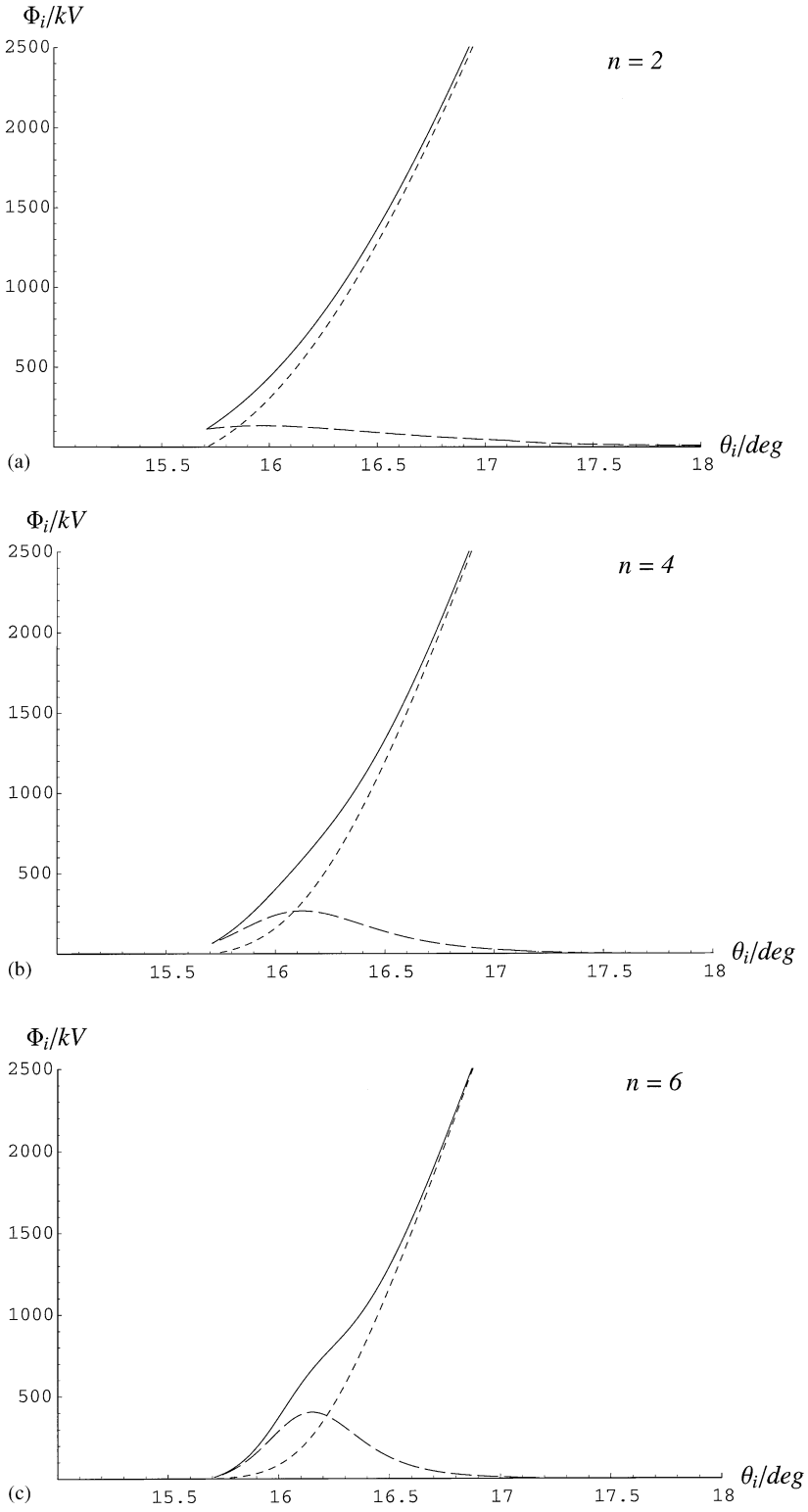

Fig. 10. Plots showing the ionospheric potential Φ_i versus co-latitude θ_i, for $n = 2, 4$, and 6 in the panels (a), (b), and (c), respectively. In each case the short-dashed lines show the equatorial potential Φ_e given by Eq. (41) mapped into the ionosphere using the constancy of F along field lines. The long-dashed lines show the field-aligned potential as in Fig. 8a. The total ionospheric potential is the sum of these two, and is shown by the solid lines.

along the jovian polar field lines, typically to altitudes above $\sim$3–4R_J. Three implications follow. The first is that the auroral primary electrons will be of high energy, $\sim$100 keV, much higher than would be expected on the basis of in situ magnetospheric observations. This is consistent with deep penetration of the jovian atmosphere and low-altitude

auroras, as observed (Ajello et al., 1998; Prangé et al., 1998; Vasavada et al., 1999). Second, the precipitating electron energy fluxes are amplified relative to those anticipated for strong diffusion precipitation of magnetospheric electrons by factors of $\sim 10^3$–10^4, to peak values of 0.1–1 W m^{-2}. These are comparable to the largest values deduced from auroral observations, as discussed in the introduction, and are sufficient to produce the brightest of observed auroras, in the range 1–10 MR (e.g. Prangé et al., 1998). Third, the free energy associated with the electron beams may be expected to excite a variety of waves in the auroral plasma. In particular, radio waves excited at frequencies near the local electron cyclotron frequency by the cyclotron maser instability in the extended acceleration region will form sources of broad-band emission extending from $\sim$100 kHz to $\sim$20 MHz. These waves correspond to the bKOM, HOM, and non-Io-DAM emissions (e.g. Zarka, 1998). We also note that the acceleration regions may be expected to produce upward-directed ionospheric ion beams which will be injected directly into the magnetosphere at energies $\sim$100 keV.

A number of important implications follow from the results derived here. The first concerns the expected nature of the response of the main auroral oval emissions, and the associated radio emissions, to the conditions prevailing in the interplanetary medium. At Earth, the main auroral emissions are related principally to the direction of the interplanetary magnetic field (IMF), which modulates the magnetosphere–ionosphere current systems associated with Dungey-cycle flow via the rate of reconnection at the magnetopause. Auroral emissions associated with the enforcement of corotation current system, however, will not behave in this manner, but will respond instead to the dynamic pressure of the solar wind which modulates the size of the magnetospheric cavity. Specifically, we expect that the emissions will generally be weaker for large values of the dynamic pressure, resulting in a compressed magnetosphere, and stronger for small values of the dynamic pressure, resulting in an expanded magnetosphere. Suppose, for example, that we initially have an expanded sub-corotational magnetosphere, and that the system is suddenly compressed by an increase in dynamic pressure of the solar wind. As the magnetospheric flux tubes move inwards, the angular velocity of the plasma will increase towards corotational values due to conservation of angular momentum. This will directly reduce the current flowing in the magnetosphere–ionosphere coupling circuit, and will cause the main oval auroras and associated radio emissions generally to weaken. In extreme cases, however, it may even be possible for the magnetospheric plasma to super-rotate for some interval in the outer regions after compression, resulting in a reversal in the sense of the current system in that region. In such cases a latitudinal restructuring of the main oval emissions will occur depending upon the new angular velocity profile, which could even involve bifurcated auroral structures if the profile becomes non-monotonic with distance. Similarly, suppose that the magnetosphere is in a compressed state, and suddenly expands outwards due to a drop in the dynamic pressure of the solar wind. Then the angular velocity of the magnetospheric plasma will drop as it expands outwards, the coupling currents will increase, and with them the brightness of the auroras and associated radio emissions. Such time-dependent phenomena may prove to be quite dramatic at Jupiter due to the large and rapid changes in solar wind dynamic pressure which occur, which are associated with interplanetary corotating interaction regions. The size of the jovian magnetosphere is known to change by linear factors of at least two due to these variations. Observations of the behaviour of the auroras may then provide a means of remote sensing the dynamic response of the middle magnetosphere to such compressions and expansions. The time-scale for re-structuring of the flow and auroras will typically be a few hours, given the time taken by the solar wind to propagate around the near-planet magnetosphere, and the internal times required for communication between the equatorial plasma and the ionosphere via Alfvén waves.

Although the time-dependent phenomena anticipated above may prove to be the most dramatic, we also expect the basic conclusion of stronger main oval auroras for expanded magnetospheres and weaker main oval auroras for compressed magnetospheres to hold under more general conditions, including the steady state. As indicated by the above analysis (Eqs. (15) and (24)), the strength of the ionospheric field-aligned currents, and the luminosity of the consequent auroras, depends both on the structure of the magnetic field in the middle magnetosphere, and on the angular velocity profile of the equatorial plasma (the dependence on the effective Pedersen conductivity will be commented upon below). In the steady state, the angular velocity profile is in principle determined self-consistently by considering the ionospheric torque on the outwardly-diffusing iogenic plasma, as in the study by Hill (1979). It may be considered a weakness of the present work that a simple empirical model of the flow was imposed, rather than being calculated self-consistently, but this at least has allowed us to choose a profile that is in rough accord with (albeit limited) plasma observations, and so to decouple this part of the theoretical problem. In Hill's analysis, the angular velocity profile was calculated assuming a dipole magnetic field. More recently, however, Pontius (1997) has solved the same problem using realistic models of the extended middle magnetosphere field lines, and has shown that the angular velocity profile is remarkably insensitive to the magnetic model (see his Fig. 4). If this is the case, then the largest effect on the magnitude of the ionospheric field-aligned currents, and hence on the auroral luminosity, will be through the field structure factor $(F_e/\rho_e^2|B_{ze}|)$. The effect of this on our results can be seen directly in Fig. 3b, where we showed the profiles of $(j_{||}/B)$ derived using the same equatorial flow profiles for both our empirical model of the extended middle magnetosphere field, and for a dipole field. The field-aligned current densities in the ionosphere implied by these results are more

than an order of magnitude larger for the extended current sheet field than for the dipole field, with the implication that the consequent auroras will be around two orders of magnitude brighter. Although this represents a comparison of extreme cases, we can nevertheless conclude that the ionospheric field-aligned current densities will generally be larger in more expanded magnetospheres with extended field lines than in compressed magnetospheres, such that the auroras will also be brighter in the former case than the latter.

Knowledge that the jovian main auroral oval maps into the sub-corotating middle magnetosphere, at distances between $\sim 20 R_J$ and several tens of R_J, also has some useful implications for the origins of adjacent auroral emissions. Specifically, we may infer that those which occur at higher latitudes, such as the transpolar emission and diffuse polar cap emissions described, e.g. by Prangé et al. (1998), are located on field lines which lie outside the main sub-corotating middle magnetosphere, and thus map to the outer magnetosphere, magnetopause boundary layers, and magnetic tail. These auroras may thus contain components which relate both to external and to internal dynamical processes, e.g: to solar wind-magnetosphere coupling (which may thus be modulated by the direction of the IMF), and to the iogenic plasma mass-loss process such as the plasmoid mechanism discussed by Vasyliunas (1983). On the lower latitude side, the emissions map from the inner middle magnetosphere, roughly inside $\sim 20 R_J$, to the Io plasma torus at $\sim 6 R_J$. Continuous relatively weak emission between the main oval and Io's orbit, referred to as the "low-latitude belt" by Prangé et al. (1998), most likely just represents a continuation to lower latitudes and lower intensities of the process discussed here, eventually weakening to levels comparable to those produced simply by pitch-angle diffusion of the magnetospheric plasma. The occasional existence of arc-like features in this region, however, also indicates the existence of more dynamic processes. The location of Io's orbit is well-marked, of course, by the longitudinally localised aurora observed downstream of the moon's footprint, which is produced by the direct interaction between Io and the near-corotating magnetospheric plasma. In addition to this, however, Prangé et al. (1998) also provide evidence for a more longitudinally extended narrow "Io oval", located near Io's orbit. It seems natural to suggest that this is formed by the local slowing of the flow observed in the vicinity of Io's orbit (e.g. Brown, 1994), which is due to local ion pick-up from the neutral atom tori (e.g. Pontius and Hill, 1982). This slowing will again be associated with a localised magnetosphere–ionosphere coupling current system of the same basic form as that considered here, and we may conjecture that the "Io oval" aurora is associated with the inner region of upward-directed field-aligned currents. It remains to be shown, however, that the ionospheric energy flux that would be produced by this process is consistent with the observed auroral luminosity (peaking at ~ 100 kR).

We now briefly discuss some limitations of our study. We start with the effect of dipole tilt, noting as above that our theoretical analysis assumes that the magnetic and rotational axes are co-aligned, as seems appropriate for an initial calculation. We may then enquire whether any systematic System III-related effects are likely to be present in the auroral luminosity, due, e.g. to the fact that for a tilted dipole, a given magnetic shell mapping to a given magnetic latitude will have differing jovigraphic latitudes at differing System III longitudes. Our initial conclusion is that no such simple systematic effect should exist. The ionospheric Pedersen current, and hence the field-aligned current, is determined by the magnetospheric flow in the atmosphere rest frame, and so assuming for simplicity that the atmosphere rigidly corotates, it is simplest to consider the issue in the planet's rest frame. In this frame the magnetic axis is fixed in direction, and departures from corotation occur as rotations of the flux shells specifically about the magnetic axis, which for sub-corotation will be directed clockwise as viewed from above the north pole. The ionospheric currents, and consequently the field-aligned currents and aurora, will thus also be axisymmetric about the magnetic axis. Correspondingly, the torque on the plasma and on the atmosphere will always be aligned with the magnetic axis, irrespective of the relative direction of the planet's spin axis. Indeed, the theory we have derived follows through exactly as above, with the identification that the factor $(\Omega_J - \omega)$ represents the angular velocity of the flux shell about the magnetic axis in the planet's rest frame. No simple System III-related longitude asymmetries associated with dipole tilt are thus anticipated. However, this statement does not preclude the existence of more subtle effects associated with non-dipole terms of the planetary field, nor effects associated with corotation breakdown of the neutral atmosphere in the Pedersen conducting layer, whose zonal flow will not then be co-aligned with the ionospheric flow. We note that Prangé et al. (1998) do indeed report some evidence for System III-related variations in the main oval emissions, but theoretical examination of these effects requires a much more detailed study than is possible here.

A far more serious limitation of our calculations, in our view, is the lack of a fully self-consistent treatment of the currents, conductivities, electric fields, and flows associated with the auroral acceleration region. In our study we took a simple empirical model of the equatorial flow, mapped it along model magnetic field lines into the ionosphere, calculated the ionospheric current and the field-aligned current assuming a uniform ionospheric conductivity, and then determined the field-aligned voltage from Knight's relation. As noted above in Section 3, this procedure ignores both the expected modulation of the ionospheric conductivity due to the precipitated particle flux, as well as the modification of the ionospheric flow and current resulting from the effect of the field-aligned voltage. While the estimates presented here should provide an initial guide to the orders involved, determination of a fully self-consistent model is a goal which requires a much more detailed calculation. In addition, the analysis should finally be closed via the self-consistent

calculation of the radial profile of the plasma angular velocity for a given mass outflow rate. However, we suggest in the latter regard that the mechanism discussed here may well provide a simple explanation for the failure of the standard theory to account for the observed slow fall-off of the plasma angular velocity with distance, a difficulty which has been discussed previously by Pontius (1997). This suggestion arises from the fact that the electron precipitation associated with the field-aligned currents which occur as the departure from rigid corotation takes place will act to increase the ionospheric conductivity, as noted above. This in turn will act to increase the torque on the equatorial plasma supplied from the ionosphere, and hence reduce the fall-off rate of the angular velocity. A detailed calculation is again required to determine whether the mechanism can account quantitatively for the observations.

Finally we note that the processes discussed here for the jovian environment should also be operative in the rotation-dominated magnetosphere of Saturn. We note that UV observations of Saturn using the Hubble Space Telescope indeed confirm the existence of a high-latitude auroral ring which appears similar in form to the main jovian oval (Trauger et al., 1998). However, in this case the auroras have an apparently persistent maximum in intensity in the dawn sector, and are of very variable intensity. A solar wind-related generation mechanism for at least some of the high-latitude auroral emission should not therefore be ruled out at this stage, noting that "region-1" currents associated with the Dungey cycle will be upward-directed in the dawn sector at Saturn due to the reversed field direction relative to Earth. Further study of the kronian auroras is required to address this issue.

The main conclusion of our paper is, however, that the principal characteristics of the main jovian auroral oval can be accounted for by the hypothesis that it is connected with the magnetosphere–ionosphere coupling currents associated with the breakdown of corotation in the middle magnetosphere, specifically with the region of upward field-aligned current. These auroral characteristics include the continuity in local time, the latitudinal location, the latitudinal width, the energy of the auroral primaries, and the precipitating energy flux and auroral luminosity. The theory also potentially provides a direct link with major aspects of non-Io-related jovian radio emissions, and with features of the radial profile of the angular velocity of the equatorial plasma. It also suggests that interplanetary modulation of the emissions should be linked primarily to the dynamic pressure of the solar wind, rather than, e.g. to the direction of the IMF, as at Earth.

Acknowledgements

EJB was supported during this study by a PPARC Quota Studentship.

References

Achilleos, N., Miller, S., Tennyson, J., Aylward, A.D., Mueller-Wodarg, I., Rees, D., 1998. JIM: a time-dependent, three-dimensional model of Jupiter's thermosphere and ionosphere. J. Geophys. Res. 103, 20,089.

Acuña, M.H., Behannon, K.W., Connerney, J.E.P., 1983. Jupiter's magnetic field and magnetosphere. In: Dessler, A.J. (Ed.), Physics of the Jovian Magnetosphere. Cambridge University Press, Cambridge, UK, p. 1.

Ajello, J., Shemansky, D., Pryor, W., Tobiska, K., Hord, C., Stephens, S., Stewart, I., Clarke, J., Simmons, K., McClintock, W., Barth, C., Gebben, J., Miller, D., Sandel, W., 1998. Galileo orbiter ultraviolet observations of Jupiter aurora. J. Geophys. Res. 103, 20,125.

Antonova, E.E., Stepanova, M.V., Vikhreva, E.A., Ovchinnikv, I.L., Teltzov, M.V., 1999. Generation of unmagnetized motion of plasma sheet electrons and its possible causes. J. Geophys. Res. 104, 19,941.

Belcher, J.W., 1983. The low-energy plasma in the jovian magnetosphere. In: Dessler, A.J. (Ed.), Physics of the Jovian Magnetosphere. Cambridge University Press, Cambridge, UK, p. 68.

Brown, M.E., 1994. Observations of mass loading in the Io plasma torus. Geophys. Res. Lett. 21, 847.

Bosqued, J.M., Maurel, C., Sauvaud, J.A., Kovrazhkin, R.A., Galperin, Y.I., 1986. Observations of auroral electron inverted-V structures by the AUREOL-3 satellite. Planet. Space Sci. 34, 255.

Bunce, E.J., Cowley, S.W.H., 2001. Divergence of the equatorial current in the dawn sector of Jupiter's magnetosphere: analysis of Pioneer and Voyager magnetic field data Planet. Space Sci. 49 (this issue).

Clarke, J.T., Ballester, G., Trauger, J., Ajello, J., Pryor, W., Tobiska, K., Connerney, J.E.P., Gladstone, G.R., Waite Jr., J.H., Ben Jaffel, L., Gérard, J.-C., 1998. Hubble Space Telescope imaging of Jupiter's UV aurora during the Galileo orbiter mission. J. Geophys. Res. 103, 20,217.

Connerney, J.E.P., 1981. Comment on 'Azimuthal magnetic field at Jupiter' by J.L. Parish, C.K. Goertz, and M.F. Thomsen. J. Geophys. Res. 86, 7796.

Connerney, J.E.P., Acuña, M.H., Ness, N.F., 1981. Modeling the Jovian current sheet and inner magnetosphere. J. Geophys. Res. 86, 8370.

Connerney, J.E.P., Acuña, M.H., Ness, N.F., Satoh, T., 1998. New models of Jupiter's magnetic field constrained by the Io flux tube footprint. J. Geophys. Res. 103, 11,929.

Dors, E.E., Kletzing, C.A., 1999. Effects of suprathermal tails on auroral electrodynamics. J. Geophys. Res. 104, 6783.

Dougherty, M.K., Southwood, D.J., Balogh, A., Smith, E.J., 1993. Field-aligned currents in the jovian magnetosphere during the Ulysses Flyby Planet. Space. Sci. 41, 29.

Edwards, T.M., Bunce, E.J., Cowley, S.W.H., 2000. A note on the vector potential of Connerney et al.'s model of the equatorial current sheet in Jupiter's magnetosphere. Planet. Space Sci. 49 (this issue).

Evans, D.S., 1974. Precipitating electron fluxes formed by a magnetic field-aligned potential difference. J. Geophys. Res. 79, 2853.

Gérard, J.-C., Dols, V., Prangé, R., Paresce, F., 1994. The morphology of the north jovian ultraviolet aurora observed with the Hubble Space Telescope. Planet. Space Sci. 42, 905.

Haerendel, G., Frey, H.U., Bauer, O.H., Rieger, E., Clemmons, J., Boehm, M.H., Wallis, D.D., Lühr, H., 1994. Inverted-V events simultaneously observed with the Freja satellite and from the ground. Geophys. Res. Lett. 21, 1891.

Hill, T.W., 1979. Inertial limit on corotation. J. Geophys. Res. 84, 6554.

Hill, T.W., Dessler, A.J., Goertz, C.K., 1983. Magnetospheric models. In: Dessler, A.J. (Ed.), Physics of the Jovian Magnetosphere. Cambridge University Press, Cambridge, UK, p. 353.

Huang, T.S., Hill, T.W., 1989. Corotation lag of the jovian atmosphere, ionosphere and magnetosphere. J. Geophys. Res. 94, 3761.

Iijima, T., Potemra, T.A., 1978. Large-scale characteristics of field-aligned currents associated with substorms. J. Geophys. Res. 83, 599.

Isbell, J., Dessler, A.J., Waite Jr. J.H., 1984. Magnetospheric energization by interaction between planetary spin and the solar wind. J. Geophys. Res. 89, 10,716.

Kane, M., Mauk, B.H., Keath, E.P., Krimigis, S.M., 1995. Hot ions in Jupiter's magnetodisc: a model for Voyager-2 low-energy charged particle measurements. J. Geophys. Res. 100, 19,473.

Kennel, C.F., Coroniti, F.V., 1975. Is Jupiter's magnetosphere like a pulsar's or Earth's?. In: Formisano, V. (Ed.), The Magnetospheres of the Earth and Jupiter. D. Reidel Publ. Co., Dordrechts Holland, p. 451.

Khurana, K.K., Kivelson, M.G., 1993. Inference of the angular velocity of plasma in the jovian magnetosphere from the sweepback of magnetic field. J. Geophys. Res. 98, 67.

Knight, S., 1973. Parallel electric fields. Planet. Space Sci. 21, 741.

Kopp, A., Birk, G.T., Otto, A., 1998. On the formation of Io-induced acceleration regions related to jovian aurora. Planet. Space Sci. 46, 405.

Ladreiter, H.P., Zarka, P., Lecacheux, A., 1994. Direction-finding study of jovian hectometric and broad-band kilometric radio emission: evidence for their auroral origins. Planet. Space Sci. 42, 919.

Laxton, N.F., Balogh, A., Cowley, S.W.H., Dunlop, M.W., Forsyth, R.J., Hynds, R.J., Staines K., 1997. Origins of the first-order anisotropy of $\sim$1 MeV protons in the Jovian magnetosphere during Ulysses flyby: flux gradients and plasma flows. Planet. Space Sci. 45, 1143.

Lu, G., Reiff, P.H., Burch, J.L., Wnningham, J.D., 1991. On the auroral current-voltage relationship. J. Geophys. Res. 96, 3523.

Lundin, R., Sandahl, I., 1978. Some characteristics of the parallel electric field acceleration of electrons over discrete auroral arcs as observed from two rocket flights. Symposium on European Rocket Research, ESA SP-135, p. 125.

Lyons, L.R., Evans, D.S., Lundin, R., 1979. An observed relation between magnetic field-aligned electric fields and downward energy fluxes in the vicinity of auroral forms. J. Geophys. Res. 84, 457.

Nagy, A.F., Barakat, A.R., Schunk, R.W., 1986. Is Jupiter's ionosphere a significant plasma source for its magnetosphere?. J. Geophys. Res. 91, 351.

Olsson, A., Eriksson, A.I., Janhunen, P., 1996. On the current-voltage relationship in auroral breakups and westwards-travelling surges. Ann. Geophys. 14, 1265.

Phillips, J.L., Bame, S.J., Barraclough, B.L., McComas, D.J., Forsyth, R.J., Canu, P., Kellogg, P.J., 1993. Ulysses plasma electron observations in the Jovian magnetosphere. Planet. Space Sci. 41, 877.

Pierrard, V., 1996. New model of magnetospheric current-voltage relationship. J. Geophys. Res. 101, 2669.

Pontius Jr., D.H., 1997. Radial mass transport and rotational dynamics. J. Geophys. Res. 102, 7137.

Pontius Jr., D.H., Hill, T.W., 1982. Departure from corotation of the Io plasma torus: local plasma production. Geophys. Res. Lett. 9, 1321.

Prangé, R., Rego, D., Pallier, L., Connerney, J.E.P., Zarka, P., Queinnec, J., 1998. Detailed study of FUV jovian auroral features with the post-COSTAR HST faint object camera. J. Geophys. Res. 103, 20,195.

Sands, M.R., McNutt, R.L., 1988. Plasma bulk flow in Jupiter's dayside middle magnetosphere. J. Geophys. Res. 93, 8502.

Satoh, T, Connerney, J.E.P., Baron, R., 1996. Emission source model of Jupiter's H3+ aurorae: a generalized inverse analysis of images Icarus 122, 1.

Scudder, J.D., Sittler Jr., E.C., Bridge, H.S., 1981. A survey of the plasma electron environment of Jupiter: a view from Voyager. J. Geophys. Res. 86, 8157.

Shiokawa, K., Fukunishi, H., Yamagishi, H., Miyaoka, H., Fujii, R., Tohyama, F., 1990. Rocket observations of the magnetosphere–ionosphere coupling processes in quiet and active arcs. J. Geophys. Res. 95, 10,679.

Shiokawa, K., Baumjohann, W., Haerendel, G., Fukunishi, H., 2000. High- and low-altitude observations of adiabatic parameters associated with auroral electron acceleration. J. Geophys. Res. 105, 2541.

Smith, E.J., Davis Jr., L., Jones, D.E., 1976. Jupiter's magnetic field and magnetosphere. In: Gehrels, T. (Ed.), Jupiter. University of Arizona Press, Tucson, p. 788.

Stauning, P., 1998. Substorm modeling based on observations of an intense high-latitude absorption surge event. J. Geophys. Res. 103, 26,433.

Swartz, W.E., Reed, R.W., McDonough, T.R., 1975. Photoelectron escape from the ionosphere of Jupiter. J. Geophys. Res. 80, 495.

Thorne, R.M., 1983. Microscopic plasma processes in the jovian magnetosphere. In: Dessler, A.J. (Ed.), Physics of the Jovian Magnetosphere. Cambridge University Press, Cambridge, UK, p. 454.

Trauger, J.T., Clarke, J.T., Ballester, G.E., Evans, R.W., Burrows, C.J., Crisp, D., Gallagher III, J.S., Griffiths, R.E., Hester, J.J., Hoessel, J.G., Holzmann, J.A., Krist, J.E., Mould, J.R., Sahai, R., Scowen, P.A., Stapelfeldt, K.R., Watson, A.M., 1998. Saturn's hydrogen aurora: wide field and planetary camera 2 imaging from the Hubble Space Telescope. J. Geophys. Res. 103, 20,237.

Tsurutani, B.T., Arballo, J.K., Goldstein, B.E., Ho, C.M., Lakhina, G.S., Smith, E.J., Cornilleau-Wherlin, N., Prangé, R., Lin, N., Kellogg, P., Phillips, J.L., Balogh, A., Krupp, N., Kane, M., 1997. Plasma wave characteristics of the jovian magnetopause boundary layer: relationship to the jovian aurora?. J. Geophys. Res. 102, 4751.

Vasavada, A.R., Bouchez, A.H., Ingersoll, A.P., Little, B., Anger, C.D., 1999. Jupiter's visible aurora and Io footprint. J. Geophys. Res. 104, 27,133.

Vasyliunas, V.M., 1983. Plasma distribution and flow. In: Dessler, A.J. (Ed.), Physics of the Jovian Magnetosphere. Cambridge University Press, Cambridge, UK, p. 395.

Weimer, D.R., Gurnett, D.A., Goertz, C.K., Menietti, J.D., Burch, J.L., Sugiura, M., 1987. The current-voltage relationship in auroral current sheets. J. Geophys. Res. 92, 18.

Zarka, P., 1998. Auroral radio emissions at the outer planets: observations and theories. J. Geophys. Res. 103, 20,159.